very-low-calorie diet, a low-calorie diet, or restricted normal food: observational cohort study. *Am J Clin Nutr* 2012;96(5):953-961.

11. Russell-Jones D, Khan R. Insulin-associated weight gain in diabetes–causes, effects and coping strategies. *Diabetes Obes Metab* 2007;9(6):799-812.
12. UK Prospective Diabetes Study (UKPDS) Group. Intensive blood-glucose control with sulphonylureas or insulin compared with conventional treatment and risk of complications in patients with type 2 diabetes (UKPDS 33). *Lancet* 1998; 352(9131):837-853.
13. Price DW, Ma Y, Rubin RR, et al.; Diabetes Prevention Program Research Group. Depression as a predictor of weight regain among successful weight losers in the diabetes prevention program. *Diabetes Care* 2013;36(2):216-221.
14. Iizuka Y, Ohashi K, Tsukamoto K, Ueki K, Kadowaki T. Education and management of diabetes at The University of Tokyo Hospital. *J Diabetes* 2011;3(2): 104-108.
15. Yamada T, Kiuchi Y, Nemoto M, Yamashita S. Charting weight four times daily as an effective behavioural approach to obesity in patients with type 2 diabetes. *Diab Vasc Dis Res* 2014;11(2):118-120.
16. Fujimoto K, Sakata T, Etou H, et al. Charting of daily weight pattern reinforces maintenance of weight reduction in moderately obese patients. *Am J Med Sci* 1992; 303(3):145-150.
17. The Japan Diabetes Society. *Food Exchange Lists-Dietary Guidance for Persons with Diabetes*. Bunkyo-do: The Japan Diabetes Society; 2002.
18. American Diabetes Association. Diagnosis and classification of diabetes mellitus. *Diabetes Care* 2013;36 Suppl 1:S67-S74.
19. Locke EA, Latham GP. Building a practically useful theory of goal setting and task motivation. *A 35-year odyssey. Am Psychol* 2002;57(9):705-717.
20. Kanfer FH, Karoly P. Self-control: a behavioristic excursion into the lion's den. *Behav Ther* 1972;3:398-416.
21. Linde JA, Jeffery RW, French SA, Pronk NP, Boyle RG. Self-weighing in weight gain prevention and weight loss trials. *Ann Behav Med* 2005;30(3):210-216.
22. Raynor HA, Jeffery RW, Ruggiero AM, Clark JM, Delahanty LM; Look AHEAD (Action for Health in Diabetes) Research Group. Weight loss strategies associated with BMI in overweight adults with type 2 diabetes at entry into the Look AHEAD (Action for Health in Diabetes) trial. *Diabetes Care* 2008;31(7):1299-1304.

J Struct Funct Genomics (2015) 16:11–23
DOI 10.1007/s10969-014-9192-z

Expression, purification, crystallization, and preliminary X-ray crystallographic studies of the human adiponectin receptors, AdipoR1 and AdipoR2

Hiroaki Tanabe · Kanna Motoyama · Mariko Ikeda · Motoaki Wakiyama · Takaho Terada · Noboru Ohsawa · Toshiaki Hosaka · Masakatsu Hato · Yoshifumi Fujii · Yoshihiro Nakamura · Satoshi Ogasawara · Tomoya Hino · Takeshi Murata · So Iwata · Miki Okada-Iwabu · Masato Iwabu · Kunio Hirata · Yoshiaki Kawano · Masaki Yamamoto · Tomomi Kimura-Someya · Mikako Shirouzu · Toshimasa Yamauchi · Takashi Kadowaki · Shigeyuki Yokoyama

Received: 18 September 2014 / Accepted: 19 November 2014 / Published online: 10 January 2015

Abstract The adiponectin receptors (AdipoR1 and AdipoR2) are membrane proteins with seven transmembrane helices. These receptors regulate glucose and fatty acid metabolism, thereby ameliorating type 2 diabetes. The full-length human AdipoR1 and a series of N-terminally truncated mutants of human AdipoR1 and AdipoR2 were expressed in insect cells. In small-scale size exclusion chromatography, the truncated mutants AdipoR1Δ88 (residues 89–375) and AdipoR2Δ99 (residues 100–386) eluted mostly in the intact monodisperse state, while the others eluted primarily as aggregates. However, gel filtration chromatography of the large-scale preparation of the tag-affinity-purified AdipoR1Δ88 revealed the presence of an excessive amount of the aggregated state over the intact state. Since aggregation due to contaminating nucleic acids may have occurred during the sample concentration step, anion-exchange column chromatography was performed immediately after affinity chromatography, to separate the intact AdipoR1Δ88 from the aggregating species. The

H. Tanabe · K. Motoyama · M. Ikeda · M. Wakiyama · T. Terada · N. Ohsawa · T. Hosaka · M. Hato · Y. Fujii · Y. Nakamura · T. Murata · S. Iwata · T. Kimura-Someya · M. Shirouzu · S. Yokoyama (✉)
RIKEN Systems and Structural Biology Center, 1-7-22 Suehiro-cho, Tsurumi-ku, Yokohama 230-0045, Japan
e-mail: yokoyama@riken.jp

H. Tanabe · S. Yokoyama
Department of Biophysics and Biochemistry and Laboratory of Structural Biology, Graduate School of Science, The University of Tokyo, Hongo, Bunkyo-ku, Tokyo 113-0033, Japan

H. Tanabe · M. Ikeda · M. Wakiyama · N. Ohsawa · T. Hosaka · M. Hato · Y. Nakamura · T. Kimura-Someya · M. Shirouzu
Division of Structural and Synthetic Biology, RIKEN Center for Life Science Technologies, 1-7-22 Suehiro-cho, Tsurumi-ku, Yokohama 230-0045, Japan

T. Terada · Y. Fujii · S. Yokoyama
RIKEN Structural Biology Laboratory, 1-7-22 Suehiro-cho, Tsurumi-ku, Yokohama 230-0045, Japan

S. Ogasawara · T. Hino · T. Murata · S. Iwata
Department of Cell Biology, Graduate School of Medicine, Kyoto University, Yoshida-Konoe-cho, Sakyo-ku, Kyoto 606-8501, Japan

T. Hino · T. Murata · S. Iwata
JST, Research Acceleration Program, Membrane Protein Crystallography Project, Yoshida-Konoe-cho, Sakyo-ku, Kyoto 606-8501, Japan

T. Murata
Department of Chemistry, Graduate School of Science, Chiba University, Yayoi-cho, Inage, Chiba 263-8522, Japan

S. Iwata
Division of Molecular Biosciences, Membrane Protein Crystallography Group, Imperial College, London SW7 2AZ, UK

S. Iwata
Diamond Light Source, Harwell Science and Innovation Campus, Chilton, Didcot, Oxfordshire OX11 0DE, UK

S. Iwata · K. Hirata · Y. Kawano · M. Yamamoto
RIKEN SPring-8 Center, Harima Institute, Kouto, Sayo, Hyogo 679-5148, Japan

M. Okada-Iwabu · M. Iwabu · T. Yamauchi (✉) · T. Kadowaki (✉)
Department of Diabetes and Metabolic Diseases, Graduate School of Medicine, The University of Tokyo, Hongo, Bunkyo-ku, Tokyo 113-0033, Japan
e-mail: tyamau-tky@umin.net

separated intact AdipoR1Δ88 did not undergo further aggregation, and was successfully purified to homogeneity by gel filtration chromatography. The purified AdipoR1Δ88 and AdipoR2Δ99 proteins were characterized by thermostability assays with 7-diethylamino-3-(4-maleimidophenyl)-4-methyl coumarin, thin layer chromatography of bound lipids, and surface plasmon resonance analysis of ligand binding, demonstrating their structural integrities. The AdipoR1Δ88 and AdipoR2Δ99 proteins were crystallized with the anti-AdipoR1 monoclonal antibody Fv fragment, by the lipidic mesophase method. X-ray diffraction data sets were obtained at resolutions of 2.8 and 2.4 Å, respectively.

Keywords Membrane protein · Adiponectin receptors AdipoR1 and AdipoR2 · Purification · Antibody · Crystallization · Lipidic mesophase

Introduction

Adiponectin is an anti-diabetic and anti-atherogenic adipokine, and is exclusively expressed in adipose tissue [1–4]. Serum adiponectin levels are significantly reduced in patients with obesity, metabolic syndrome, and type 2 diabetes [5]. We previously reported the expression cloning of complementary DNAs encoding adiponectin receptors (*Adipor*) 1 and 2 [6]. These adiponectin receptors, AdipoR1 and AdipoR2, are key membrane proteins that exert anti-metabolic syndrome effects. Adiponectin accomplishes its biological effects by binding to the AdipoR1 and AdipoR2 receptors. In the liver, both adiponectin receptors mediate the major part of the insulin-sensitizing actions of adiponectin, while AdipoR1 primarily does so in skeletal muscle. AdipoR1 and AdipoR2 regulate glucose and fatty acid metabolism partly via the activation of the AMPK [7–9], Ca^{2+} [10], and PPARα [11, 12] signaling pathways. Interestingly, AdipoR1 and AdipoR2 are predicted to contain seven-transmembrane domains [6], but they are structurally distinct from G-protein coupled receptors (GPCRs) [13]. The adiponectin receptors possess an internal N-terminus and an external C-terminus, which is opposite to the topology of GPCRs. Therefore, AdipoRs are predicted to have unique structures, as compared to those of GPCRs.

Here, we report the expression and purification of the N-terminally truncated human AdipoR1 and AdipoR2 proteins, crystallization of the truncated AdipoR1 and AdipoR2 in complexes with the Fv fragment of an anti-AdipoR1 monoclonal antibody, and their preliminary X-ray crystallographic studies.

Materials and methods

Plasmid construction

The *Bgl*II-FLAG-TEV-*Bam*HI-*Eco*RI DNA (5′-GGAAGA TCTATGGATTACAAGGACGACGACGATAAGGAAA ACCTGTATTTTCAGGGCGGATCCGAATTCCCG-3′) and its complementary DNA were synthesized, annealed together, digested with *Bgl*II and *Eco*RI, and subcloned into the *Bam*HI and *Eco*RI sites of pFastBac1. The resulting plasmid encodes a Flag tag followed by a TEV cleavage site at the N-terminus, and is referred to as pFastBac1-FT hereafter. The cDNAs encoding the full-length human AdipoR1 (residues 1–375) and N-terminally-truncated mutants of AdipoR1 and AdipoR2 (AdipoR1Δ46, residues 47–375; Δ76, 77–375; Δ88, 89–375; Δ101, 102–375; and Δ119, 120–375; AdipoR2Δ58, residues 59–386; Δ87, 88–386; Δ99, 100–386; Δ112, 113–386; and Δ130, 131–386) were amplified by PCR. The PCR products were digested with *Bam*HI and *Xho*I for AdipoR1 and *Eco*RI and *Xho*I for AdipoR2, and then inserted into the pFastBac1-FT vector.

Protein expression in insect cells

High-titer recombinant baculoviruses were obtained with the Bac-to-Bac Baculovirus Expression System (Invitrogen), according to the manufacturer's protocol. For large-scale and small-scale production of the recombinant proteins, *Trichoplusia ni* (High Five) cells, at densities of 2×10^6 and $2–5 \times 10^6$ cell/ml, respectively, were infected with the high-titer viral stock at a multiplicity of infection (m.o.i.) of 0.5. Cells were harvested by centrifugation at 42-h post infection, and were washed once with phosphate buffer saline (PBS). Cells were flash-frozen in liquid nitrogen, and stored at −80 °C until use.

T. Kadowaki
e-mail: kadowaki-3im@h.u-tokyo.ac.jp

M. Okada-Iwabu · M. Iwabu · T. Yamauchi · T. Kadowaki
Department of Integrated Molecular Science on Metabolic Diseases, 22nd Century Medical and Research Center, The University of Tokyo, Hongo, Bunkyo-ku, Tokyo 113-0033, Japan

M. Iwabu
PRESTO, Japan Science and Technology Agency, Kawaguchi, Saitama 332-0012, Japan

T. Yamauchi
CREST, Japan Science and Technology Agency, Kawaguchi, Saitama 332-0012, Japan

Large-scale membrane preparation

For large-scale preparations of the full-length AdipoR1, AdipoR1Δ88, and AdipoR2Δ99 proteins, frozen cells were thawed in high osmotic buffer [10 mM HEPES–NaOH buffer (pH 7.4) containing 1.0 M NaCl, 10 mM $MgCl_2$, 20 mM KCl, and EDTA-free Complete Protease Inhibitor Cocktail (Roche)], and disrupted by Dounce homogenization. The raw membranes were collected by ultracentrifugation at 100,000×*g* for 30 min, and were resuspended in high osmotic buffer. These ultracentrifugation and resuspension steps were repeated four times, to remove the peripheral membrane proteins. Finally, the washed membranes were resuspended in 20 mM HEPES–NaOH buffer (pH 7.4) containing 100 mM NaCl and 10 % (v/v) glycerol, flash-frozen with liquid nitrogen, and stored at −80 °C until use. The membrane proteins were quantified with the *DC* Protein Assay (Bio-Rad), using bovine serum albumin (BSA) as the standard.

Large-scale protein purification

The purified membranes (20 mg/ml of total membrane proteins) were solubilized with 20 mM HEPES–NaOH buffer (pH 7.4) containing 100 mM NaCl, 10 % (v/v) glycerol, and 1 % (w/v) *n*-dodecyl-β-D-maltoside (DDM, Anatrace), for 1–2 h at 4 °C. The insoluble materials were removed by ultracentrifugation at 100,000×*g* for 1 h. The supernatant was filtered (0.45 μm) and incubated with Anti DYKDDDDK Tag Antibody Beads (Wako) in 20 mM HEPES–NaOH buffer (pH 7.4) containing 300 mM NaCl, 10 % (v/v) glycerol, and 0.5 % (w/v) DDM, at 4 °C with gentle agitation. The beads were washed with thirty column volumes of buffer A [20 mM HEPES–NaOH buffer (pH 7.4), containing 10 % (v/v) glycerol, 0.025 % (w/v) DDM, and 0.0001 % (w/v) cholesteryl-hemi-succinate (CHS, Anatrace)], containing 200 mM NaCl. Then, the adsorbed AdipoR1/AdipoR2 proteins were eluted with five column volumes of buffer A containing 100 or 200 mM NaCl and 0.1 mg/ml DYKDDDDK peptide (Wako). Further purification was performed by the following three methods.

First, the affinity-purified sample was concentrated by ultrafiltration with an Ultra-15 30 K-MWCO filter (Millipore), and then loaded on a HiLoad 16/600 Superdex 200 (GE Healthcare) column equilibrated in buffer A containing 200 mM NaCl. Second, the affinity-purified sample, in 100 mM NaCl, was loaded on a 1-ml HiTrap Q column (GE Healthcare) equilibrated with buffer A containing 100 mM NaCl, and was eluted by a 100–1,000 mM linear NaCl gradient in buffer A. The sample was further purified by SEC on a Superdex 200 10/300 (GE Healthcare) column, in buffer A containing 200 mM NaCl. Third, the affinity-purified sample, in 200 mM NaCl, was loaded on a 1-ml HiTrap Q column equilibrated with buffer A containing 200 mM NaCl, and the flow-through fraction was collected. The polyhistidine-tagged TEV protease was added to the anion-exchange-purified fraction, and incubated with the receptor overnight at 4 °C. The receptor was separated from TEV by adsorption to TALON resin (Clontech), and was further purified by SEC on a Superdex 200 10/300 column in buffer A containing 200 mM NaCl. The purities of the AdipoR1Δ88 and AdipoR2Δ99 proteins were assessed by SDS-PAGE.

Small-scale SEC analysis

Frozen cells were thawed in the high osmotic buffer, and then sonicated to disrupt the cells. The membranes were collected by ultracentrifugation at 100,000×*g* for 15 min, and were resuspended in 20 mM HEPES–NaOH buffer (pH 7.4) containing 150 mM NaCl, 1 mM EDTA, and 5 mM $MgCl_2$. The purified membranes (10 mg/ml of membrane protein) were solubilized with 20 mM HEPES–NaOH buffer (pH 7.4) containing 1 % (w/v) DDM, 150 mM NaCl, 1 mM EDTA, and 5 mM $MgCl_2$, for 1 h at 4 °C. The insoluble material was removed by ultracentrifugation at 100,000×*g* for 30 min. The supernatant was incubated with 100 μl anti-FLAG M2 affinity gel (Sigma) in 20 mM HEPES–NaOH buffer (pH 7.4) containing 150 mM NaCl, 1 mM EDTA, 5 mM $MgCl_2$, 5 % (v/v) glycerol, and 0.5 % (w/v) DDM, at 4 °C with gentle agitation. The beads were washed with five column volumes of 20 mM HEPES–NaOH buffer (pH 7.4) containing 150 mM NaCl, 1 mM EDTA, 5 mM $MgCl_2$, 5 % (v/v) glycerol, and 0.04 % (w/v) DDM, and the adsorbed receptor was eluted with five column volumes of the same buffer containing 0.1 mg/ml FLAG peptide (Sigma). The affinity purified sample was then loaded on a Superdex 200 10/300 column in 20 mM HEPES–NaOH buffer (pH 7.4) containing 200 mM NaCl, 10 % (v/v) glycerol, and 0.04 % (w/v) DDM. Fractions (1 ml) were collected. Portions (5 μl) of the eluates were separated by SDS-PAGE, and transferred to a PVDF membrane. The membranes were blocked in 5 % (w/v) dry milk in TBS-T buffer [Tris-buffered saline, 0.1 % (v/v) Tween-20] at room temperature for 1 h. The blocked membranes were detected with the anti-FLAG M2 monoclonal antibody (Sigma) and the anti-mouse IgG, HRP-linked whole antibody from sheep (GE Healthcare) in TBS-T buffer. The membranes were visualized using Immobilon Western Chemiluminescent HRP Substrate (Millipore), and detected with an LAS3000 imager (Fuji).

Characterization of the purified N-terminally truncated mutants of AdipoR1 and AdipoR2

The purified AdipoR1Δ88 and AdipoR2Δ99 proteins were analyzed by the following three methods. First, the thermal stabilities of AdipoR1Δ88 and AdipoR2Δ99 were analyzed by the 7-diethylamino-3-(4-maleimidophenyl)-4-methyl coumarin (CPM) assay method [14, 15]. The fluorescence of the CPM dye was measured with a 340-nm excitation filter with a 10-nm bandpass and a 460-nm emission filter with a 35-nm bandpass at 40 °C, on a FUSION α Microplate Reader PerkinElmer. Second, the lipids that co-purified with the AdipoR1Δ88 and AdipoR2Δ99 proteins were analyzed by thin layer chromatography (TLC). The full-length AdipoR1 and AdipoR2, prepared by FLAG affinity and anion-exchange chromatography, were also analyzed for comparison. The proteins were dissolved in chloroform/methanol [2:1 (v/v)], and the bound lipids were extracted from the proteins. The extracted samples were applied to a silica gel 60 TLC plate (Merck Millipore), which was then developed by a solvent system composed of chloroform/methanol/water [65:25:4 (v/v)]. The lipids were visualized with acetic acid/sulfuric acid [1:1 (v/v)], the phosphomolybdic reagent (Pierce), and the ninhydrin reagent (Wako). Third, the ligand-binding activity of AdipoR1Δ88 was measured by surface plasmon resonance (SPR) measurements. The purified AdipoR1Δ88 was reconstituted into liposomes [5 mg/ml egg yolk phosphatidylcholine (PC) (Avanti Polar Lipids Inc.) and 0.05 mg/ml biotinyl-phosphatidylethanolamine (biotinyl-PE) (Avanti Polar Lipids Inc.)], and the reconstituted liposomes were immobilized onto a sensor chip SA. Binding analyses were performed with a range of osmotin concentrations (0.5–8 μM) on a Biacore T200 (GE Healthcare).

Production of the anti-AdipoR1 monoclonal antibody

All animal experiments described here were approved by the Institutional Animal Care and Use Committee of Kyoto University Graduate School of Medicine. The purified untagged AdipoR1Δ88 was reconstituted into liposomes [5 mg/ml egg yolk PC and 1 mg/ml lipid A (Sigma)]. Female BALB/c mice were immunized five times with 0.1 mg doses of the reconstituted AdipoR1Δ88, at intervals of 10 days. Single-cell suspensions were prepared from the spleens of the immunized mice, and the cells were fused with P3U1 myeloma cells, using the conventional polyethylene glycol (PEG) method [16]. Screening of antibodies was performed by three methods, enzyme-linked immunosorbent assay (ELISA), fluorescence-detection SEC (FSEC), and denatured dot blot assays [17, Ogasawara et al., manuscript in preparation]. For ELISA, the purified AdipoR1Δ88 was reconstituted into liposomes containing biotinyl-PE, and was immobilized on Immobilizer Streptavidin plates (Nunc). High-affinity antibodies that formed stable complexes with the purified AdipoR1Δ88 were selected by FSEC, using the fluorescein-conjugated Fab fragment of an anti-mouse IgG (Jackson), on a Superdex 200 5/150 column (GE Healthcare). Antibodies that recognized the native conformation of AdipoR1Δ88 were selected by dot blot assays with SDS-denatured AdipoR1Δ88. Each selected clone was isolated by the limiting dilution-culture method, and monoclonal hybridoma cell lines producing anti-AdipoR1Δ88 antibodies were established.

Recombinant production of the Fv fragment of the anti-AdipoR1 antibody

The sequences of the V_H and V_L regions were determined by the standard method, with total RNA isolated from the hybridoma cells [18]. The cloned V_H and V_L cDNA fragments were subcloned into the TA-cloning vector, pCR2.1 TOPO (Invitrogen) [19], encoding a fusion protein with an N-terminal His-tag, a SUMO tag, and a SUMO protease cleavage site. The V_H and V_L fragments were co-synthesized by the *E. coli* cell-free protein synthesis method [20], supplemented with DsbC and the reduced and oxidized forms of glutathione (GSH and GSSG, respectively) to form disulfide bonds [21]. The reaction solution was centrifuged at 20,000×*g* and 4 °C for 10 min. The supernatant was loaded on a 1-ml HisTrap column (GE Healthcare) equilibrated with 20 mM Tris–HCl buffer (pH 8.0) containing 500 mM NaCl and 20 mM imidazole, and was eluted by a 20–500 mM linear gradient of imidazole in 20 mM Tris–HCl buffer (pH 8.0) containing 500 mM NaCl. The His- and SUMO-tags were cleaved by SUMO protease for 2–3 days at room temperature, and were removed by a second passage through the HisTrap column. The protein sample was then loaded on a HiLoad 16/600 Superdex 200 column, equilibrated in 20 mM HEPES–NaOH buffer (pH 7.4) containing 200 mM NaCl. The purified Fv fragment (Fv43) was concentrated to approximately 20 mg/ml, by ultrafiltration with an Ultra-15 10 K-MWCO filter (Millipore).

Preparation of the AdipoR1·Fv43 and AdipoR2·Fv43 complexes

The Fv43 (24.8 kDa) was mixed with the purified FLAG-tagged AdipoR1Δ88 (35.0 kDa) or untagged AdipoR2Δ99 (32.9 kDa), and incubated on ice for 30 min. The mixture was loaded onto a Superdex 200 10/300 column equilibrated with 20 mM HEPES–NaOH buffer (pH 7.4) containing 200 mM NaCl, 0.025 % (w/v) DDM, and 0.0001 % (w/v) CHS, and was eluted using the same buffer. Fractions

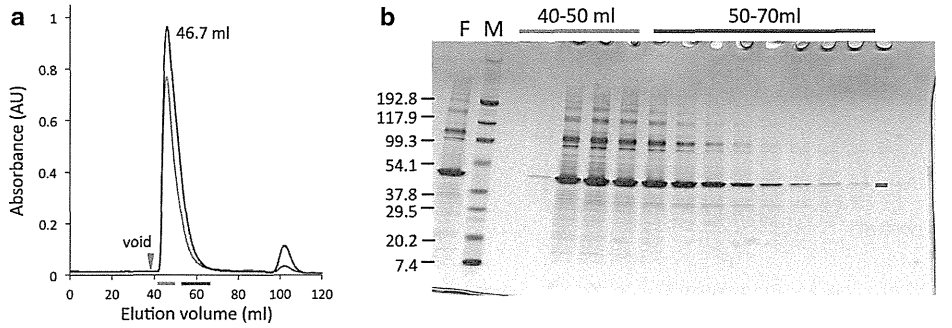

Fig. 1 Purification of full-length AdipoR1. **a** Gel filtration chromatogram of the full-length AdipoR1 expressed in High Five insect cells. The proteins were purified by FLAG-affinity chromatography, and then loaded onto a HiLoad 16/600 Superdex 200 column. The main peak retention volume is labeled in *black* (46.7 ml). The absorbances at 280 and 254 nm are colored *blue* and *red*, respectively. **b** SDS-PAGE analysis of the gel-filtration chromatographic fractions containing the full-length AdipoR1. Fractions indicated by the *orange* and *green lines* along the horizontal axis in **a** were analyzed by SDS-PAGE. *Lane F*, the eluate from FLAG-affinity chromatography; *Lane M*, molecular-weight markers (kDa)

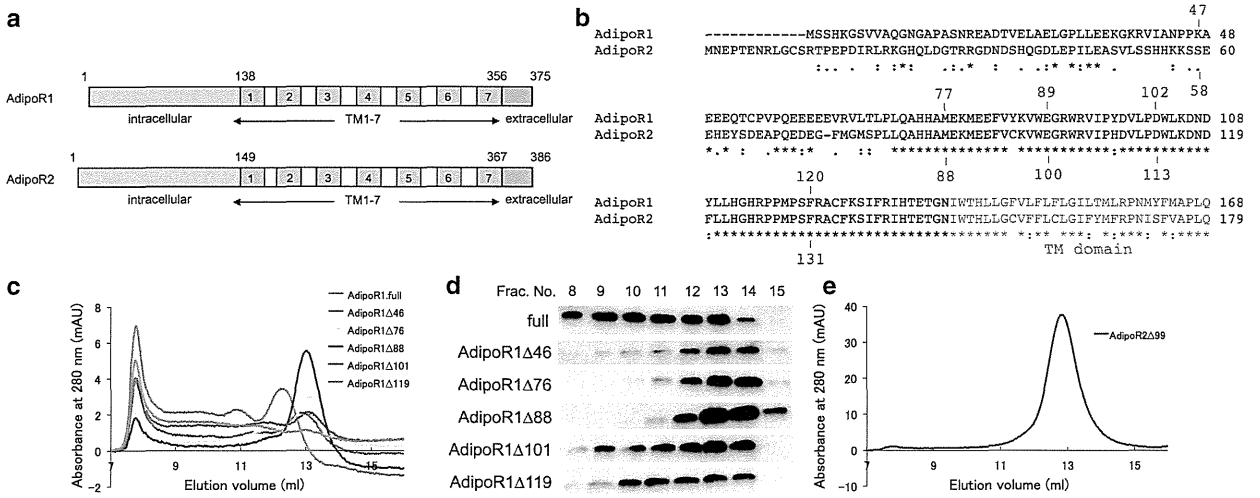

Fig. 2 Screening of the N-terminally truncated mutants of AdipoR1 and AdipoR2. Several N-terminal deletion mutants were analyzed by size-exclusion chromatography. **a** Schematic representations of human AdipoR1 (*top*) and AdipoR2 (*bottom*). **b** Amino acid sequences of the N-terminal regions of human AdipoR1 and AdipoR2. The starting amino acid residues of the N-terminally truncated mutants of AdipoR1 and AdipoR2 are numbered in *red*. Amino acids in putative transmembrane domains are shown in *gray letters*. The sequences were aligned with ClustalW [38]. **c** Size-exclusion chromatograms of the full-length form and the N-terminally truncated mutants of AdipoR1. **d** Detection of the AdipoR1 protein in the size-exclusion chromatography fractions by western blotting with the anti-FLAG M2 antibody. **e** Size-exclusion chromatogram of AdipoR2Δ99

containing the complex were collected and concentrated to approximately 15 mg/ml by ultrafiltration (Ultra-4 30 K-MWCO, Millipore). The purities of the AdipoR1Δ88·Fv43 and AdipoR2Δ99·Fv43 complexes were assessed by SDS-PAGE.

Crystallization and X-ray data collection

The purified AdipoR1Δ88·Fv43 and AdipoR2Δ99·Fv43 complexes were reconstituted into a lipidic mesophase, by mixing with molten lipid in a mechanical syringe mixer [22]. The protein-LCP mixture contained 40 % (w/w) protein solution, 54 % (w/w) monoolein (Sigma) and 6 % (w/w) cholesterol (Sigma). Forty nanoliter drops of the resulting lipidic mesophase sample were dispensed into 96 well glass plates, overlaid with 0.8 μl precipitant solution, and covered with thin cover glasses, by the use of laboratory-constructed manual and robotic micro-dispensers [23, Hato et al., manuscript in preparation]. Crystallization setups were performed at room temperature, and the plates were incubated at 20 °C. Crystals were harvested directly from the lipidic mesophase using MiTeGen micromounts, and flash cooled in liquid nitrogen. Data collection was performed on beamline BL32XU at SPring-8, using an MX225HE CCD detector [24–26]. X-ray diffraction data with a micro beam of 1 μm × 10 μm (horizontal × vertical) were collected at

100 K, by the helical scan method with 1° oscillation. The data from the AdipoR1Δ88·Fv43 and AdipoR2Δ99·Fv43 crystals were indexed, scaled, and merged with the HKL2000 program suite [27] and the XDS package [28], respectively.

Results and discussion

Screening of deletion mutants of AdipoR1 and AdipoR2

The full-length AdipoR1 (residues 1–375) was expressed in baculovirus-infected High Five insect cells, and the membrane fractions were prepared. Upon gel filtration chromatography (size-exclusion chromatography, SEC) on a HiLoad 16/600 Superdex 200 column, the detergent-solubilized full-length AdipoR1 mainly eluted just after the void volume (40 ml) (Fig. 1). If the full-length AdipoR1 was monomeric and monodisperse, then the proteomicelle should exhibit an estimated molecular mass of ca. 125 kDa (the full-length AdipoR1 monomer, 44.7 kDa; DDM micelle, ca. 80 kDa), and elute after 55 ml (the elution volume of ferritin, 440 kDa) on the gel filtration column. However, most of the full-length AdipoR1 eluted before 55 ml (Fig. 1), indicating that this sample was highly polydisperse and not suitable for crystallization.

We therefore tried to modify the AdipoR1 construct. Prediction servers of protein secondary structure, PSIPRED v3.3 [29], and transmembrane domains, HMMTOP [30], suggested that human AdipoR1 and AdipoR2 have a long N-terminal region, seven transmembrane (TM) helices with short loops connecting the TM helices, and a short C-terminal region (Fig. 2a). Since more than 50 % of the N-terminal region was predicted to be flexible, we speculated that this long N-terminal tail is related to the observed polydispersity of AdipoR1 (Fig. 1).

Therefore, we constructed a series of N-terminally-deleted mutants of AdipoR1 (Fig. 2b). They were expressed on a small scale, and were analyzed by SEC without concentration. In this small-scale SEC analysis of AdipoR1 (Fig. 2c, d), the non-concentrated sample of the full-length AdipoR1 was less aggregated, as compared with the concentrated sample in the large-scale preparation, because it exhibited a small peak eluting at ca. 13 ml (Fig. 1). This ca. 13-ml elution volume in the small-scale SEC analysis should correspond to ca. 65 ml in the large-scale gel filtration chromatography. Deletions of residues 1–46 (Δ46) and 1–76 (Δ76) of AdipoR1 significantly increased the fraction eluting at ca. 13 ml, as compared with the full-length AdipoR1. However, the total amounts of these deletion mutants were much lower than that of the full-length AdipoR1 obtained from the same amount of cells.

Fig. 3 Large-scale preparation of FLAG-tagged AdipoR1Δ88 and AdipoR2Δ99 expressed in High Five cells. In the chromatograms (**a**, **c–h**, **j**, **k**, **m**, **n**), the absorbances at 280 and 254 nm, and the NaCl concentration are shown in *blue*, *red*, and *light green*, respectively. **a** Gel filtration chromatogram of FLAG-tagged AdipoR1Δ88 expressed in High Five insect cells. The proteins were purified by FLAG-affinity chromatography, and then chromatographed on a HiLoad 16/600 Superdex 200 column. The main peak elution volume is labeled in *black* (58.8 ml). **b** SDS-PAGE analysis of the gel-filtration chromatographic fractions containing the FLAG-tagged AdipoR1Δ88. Fractions indicated by the *orange* and *green lines* along the horizontal axis in **a** were analyzed by SDS-PAGE. *Lane M*, molecular-weight markers (kDa). **c** Anion-exchange chromatogram of the FLAG-tagged AdipoR1Δ88, with isocratic elution by 100 mM NaCl in buffer A, and subsequently with gradient elution by 100–1,000 mM NaCl in buffer A. **d**, **e** Gel filtration chromatograms of the peak 1 (**d**) and peak 2 (**e**) fractions, indicated by the *orange* and *green lines* in **c**, respectively. **f** Anion-exchange chromatogram of the FLAG-tagged AdipoR1Δ88, with isocratic elution by 200 mM NaCl in buffer A, and subsequently with gradient elution by 200–1,000 mM NaCl in buffer A. **g**, **h** Gel filtration chromatograms of the flow-through (**g**) and adsorbed (**h**) fractions, indicated by the *orange* and *green lines* in **f**, respectively. **i** SDS-PAGE analysis of the FLAG-tagged AdipoR1Δ88. *Lane M*, molecular-weight markers (kDa); *lane 1*, the membrane fraction; *lane 2*, DDM-solubilized membrane proteins in the supernatant after ultracentrifugation; *lane 3*, the flow-through fraction from FLAG-affinity chromatography; *lane 4*, the eluate from FLAG-affinity chromatography; *lane 5*, the flow-through fraction from anion-exchange chromatography (**f**); *lanes 6–9*, the peak fractions of the FLAG-tagged AdipoR1Δ88 from gel filtration chromatography (**g**). **j** Anion-exchange chromatogram of AdipoR2Δ99, with isocratic elution by 200 mM NaCl in buffer A and subsequently with gradient elution by 200–1,000 mM NaCl in buffer A. **k** Gel filtration chromatogram of the flow-through fractions indicated by the *orange line* in **j**. **l** SDS-PAGE analysis of AdipoR2Δ99. *Lane M*, molecular-weight markers (kDa); *lane 1*, the membrane fraction; *lane 2*, DDM-solubilized membrane proteins in the ultracentrifugation supernatant; *lane 3*, the flow-through fraction from FLAG-affinity chromatography; *lane 4*, the eluate from FLAG-affinity chromatography; *lane 5*, the flow-through fraction from anion-exchange chromatography after the TEV protease digestion; *lane 6*, the flow-through fraction from TALON chromatography; *lanes 7–11*, the peak fractions of AdipoR2Δ99 from gel filtration chromatography. **m**, **n** Gel filtration chromatographic analysis of the purified FLAG-tagged AdipoR1Δ88 (**m**) and the purified AdipoR2Δ99 (**n**)

By contrast, the deletion of residues 1–88 (Δ88) of AdipoR1 further improved the monodispersity in the SEC analysis, and the total amount of this deletion mutant protein was as high as that of the full-length AdipoR1 (Fig. 2c, d). On the other hand, further deletion mutants (AdipoR1Δ101 and AdipoR1Δ119) were less aggregated than the full-length protein, but appreciably more aggregated than AdipoR1Δ88. Thus, we concluded that the AdipoR1Δ88 mutant was the best among the tested deletion mutants. The screening of AdipoR2Δ58, Δ87, Δ99, Δ112, and Δ130 was performed in the same manner, and AdipoR2Δ99 was found to be the best (Fig. 2e). Consequently, the AdipoR1Δ88 and AdipoR2Δ99 mutants were selected and used for further crystallization trials.

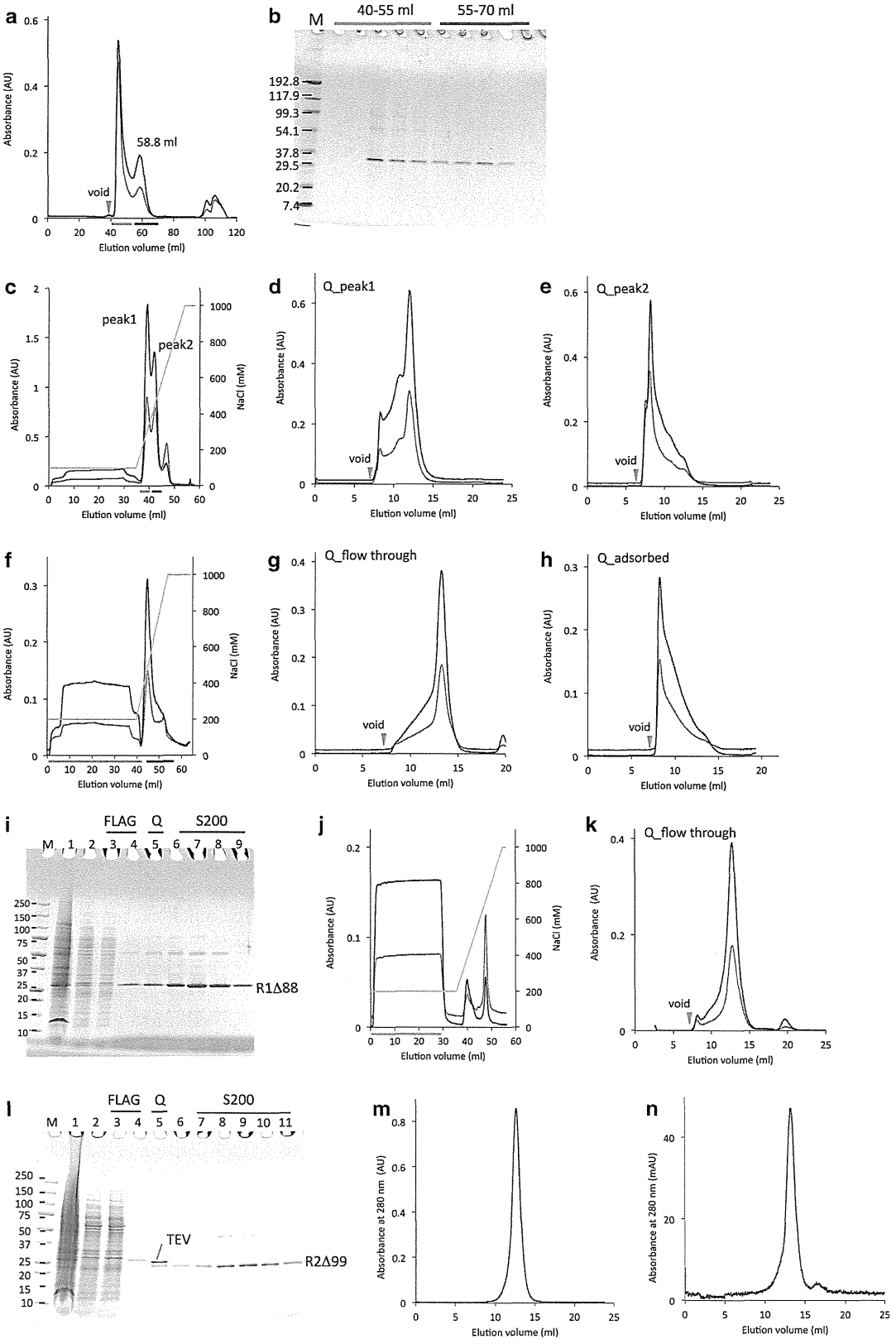
a
Absorbance (AU)
58.8 ml
void
Elution volume (ml)
b
M
40-55 ml
55-70 ml
192.8
117.9
99.3
54.1
37.8
29.5
20.2
7.4
c
peak1
peak2
Absorbance (AU)
NaCl (mM)
Elution volume (ml)
d
Q_peak1
Absorbance (AU)
void
Elution volume (ml)
e
Q_peak2
Absorbance (AU)
void
Elution volume (ml)
f
Absorbance (AU)
NaCl (mM)
Elution volume (ml)
g
Q_flow through
Absorbance (AU)
void
Elution volume (ml)
h
Q_adsorbed
Absorbance (AU)
void
Elution volume (ml)
i
FLAG
Q
S200
M 1 2 3 4 5 6 7 8 9
250
150
100
75
50
37
25
20
15
10
R1Δ88
j
Absorbance (AU)
NaCl (mM)
Elution volume (ml)
k
Q_flow through
Absorbance (AU)
void
Elution volume (ml)
l
FLAG
Q
S200
M 1 2 3 4 5 6 7 8 9 10 11
250
150
100
75
50
37
25
20
15
10
TEV
R2Δ99
m
Absorbance at 280 nm (AU)
Elution volume (ml)
n
Absorbance at 280 nm (mAU)
Elution volume (ml)

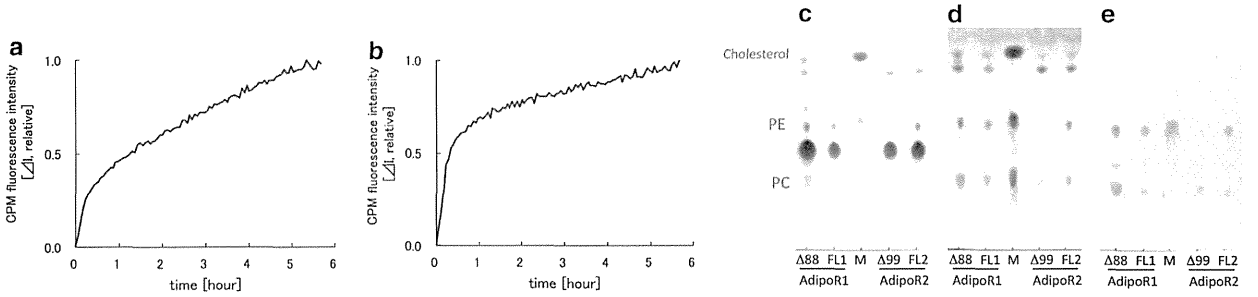

Fig. 4 Characterization of the purified AdipoR1Δ88 and AdipoR2Δ99 proteins. **a**, **b** CPM assay of AdipoR1Δ88 (**a**) and AdipoR2Δ99 (**b**). **c**–**e** TLC analysis of AdipoR1Δ88 (Δ88), the full-length AdipoR1 (FL1), AdipoR2Δ99 (Δ99), and the full-length AdipoR2 (FL2). The lipids were visualized with acetic acid/sulfuric acid [1:1 (v/v)] (**c**), the phosphomolybdic reagent (**d**), and the ninhydrin reagent (**e**). *Lane M*, polar lipid mixture (Matreya)

Large-scale preparations of N-terminally truncated AdipoR1 and AdipoR2

The FLAG-tagged AdipoR1Δ88 and AdipoR2Δ99 were overexpressed in baculovirus-infected High Five insect cells. In general, membrane proteins are purified by minimal steps of chromatography, such as one-step affinity chromatography or two-step (affinity and size-exclusion) chromatography, to avoid deterioration caused by delipidation due to excessive washing with detergents. Therefore, the FLAG-tagged AdipoR1Δ88 was partially purified by stepwise FLAG affinity chromatography, and then fractionated by gel filtration chromatography, in which the AdipoR1Δ88 eluted from the void volume (40 ml) to 70 ml, and formed two peaks (Fig. 3a, b). In this large-scale preparation, the affinity-purified AdipoR1Δ88 behaved differently in the gel filtration (Fig. 3a, b), as compared to the small-scale SEC analysis (Fig. 2c, d). The low molecular mass fraction eluting at 58.8 ml (Fig. 3a) was considered to correspond to the monodisperse fraction of AdipoR1Δ88 eluting at 13 ml in the small-scale SEC analysis. On the other hand, the high molecular mass, aggregated fraction was drastically larger in the large-scale preparation, as compared to the small-scale preparation (Figs. 2c, 3a). Therefore, the affinity-purified AdipoR1Δ88 still aggregated during the sample concentration for gel filtration chromatography, as in the case of the full-length AdipoR1 (Fig. 1), although the properties of AdipoR1 were greatly improved by the N-terminal deletion (Δ88).

Accordingly, we explored the cause of the aggregation. As compared with the monodisperse fraction, the aggregated fraction exhibited a stronger absorbance at 254 nm relative to that at 280 nm (Fig. 3a). Therefore, we hypothesized that nucleic acids contained in the FLAG-affinity-purified AdipoR1Δ88 preparation promoted protein aggregation. To quickly remove the putative nucleic acid contamination, we included an anion-exchange column chromatography step immediately after the FLAG affinity chromatography. The FLAG-tagged AdipoR1Δ88, in buffer A containing 100 or 200 mM NaCl, was applied to a 1-ml HiTrap Q column. The FLAG-tagged AdipoR1Δ88, in buffer A containing 100 mM NaCl, was adsorbed on the column and eluted at low salt concentrations (150–250 mM NaCl) (Fig. 3c–e), whereas that in buffer A containing 200 mM NaCl was eluted in the flow-through fraction (Fig. 3f–i). On the other hand, the aggregated AdipoR1Δ88 was adsorbed on the column with either 100 mM or 200 mM NaCl, and was eluted at high salt concentrations (250–400 mM NaCl) (Fig. 3c, e, f, h). Thus, we could quickly separate the "intact" FLAG-tagged AdipoR1Δ88 from the aggregated AdipoR1Δ88, in buffer A containing 200 mM NaCl, by anion-exchange chromatography (Fig. 3f, g). Once it was purified in this manner, the "intact" FLAG-tagged AdipoR1Δ88 did not undergo the fast aggregation, and was eluted as a symmetrical peak in gel filtration chromatography. In other words, the "rotten apple" (the nucleic acid-aggregated AdipoR1) can be removed quickly by the anion-exchange chromatography, before it "spoils the barrel". As the cause of the aggregation had been found, we tried another method to reduce it: the sonication of the membrane preparation was also useful for breaking up nucleic acids, and the aggregation of the receptors was significantly reduced during the purification step.

In the same manner, the affinity-purified FLAG-tagged AdipoR2Δ99, in buffer A containing 200 mM NaCl, was eluted in the flow-through fraction in the HiTrap Q column chromatography (Fig. 3j–l). The FLAG tag of AdipoR2Δ99 was removed after the HiTrap Q column chromatography. Thus, the FLAG-tagged AdipoR1Δ88 and the untagged AdipoR2Δ99 were purified to near homogeneity (Fig. 3m, n). Removing the nucleic acids during the membrane preparation and the early stages of purification was essential to obtain larger amounts of the highly homogeneous AdipoR1 and AdipoR2 proteins.

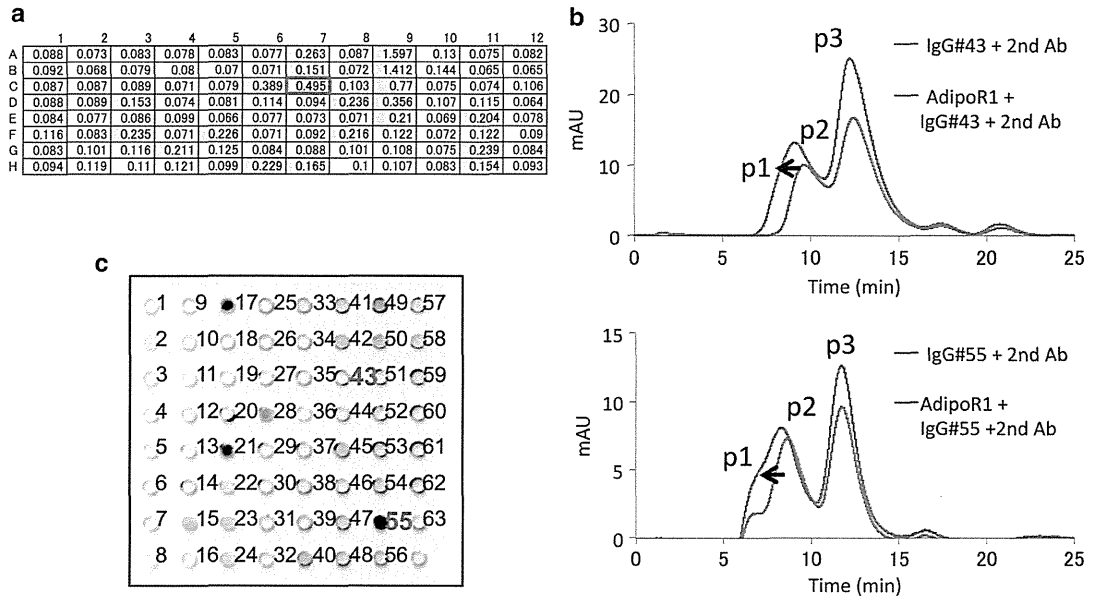

Fig. 5 Screening of anti-AdipoR1 antibodies. **a** Representative ELISA plate results. *Yellow areas* represent ELISA positive clones. Well C7, enclosed in a *red box*, indicates clone #43. **b** FSEC analyses of IgG#43 (*top*) and IgG#55 (*bottom*). Peaks *p1*, *p2*, and *p3* represent the peak of the ternary complex (AdipoR1Δ88, the antibody from hybridoma cells, and the fluorescein–Fab fragment), the antibody complex (the antibody from hybridoma cells and the fluorescein–Fab fragment), and the free fluorescein–Fab fragment, respectively. **c** SDS-denatured dot blot screening of anti-AdipoR1 antibodies. IgG#17, IgG#21, and IgG#55 stained denatured AdipoR1. IgG#43 and IgG#55 are numbered in *red*

Characterization of the purified AdipoR1Δ88 and AdipoR2Δ99 proteins

First, the stabilities of the purified AdipoR1Δ88 and AdipoR2Δ99 proteins were analyzed by the CPM assay method [14, 15] (Fig. 4a, b). When the $t_{1/2}$ value of thermal denaturation at 40 °C is 17 min or longer, the membrane protein is considered to be sufficiently stable [31]. The corresponding $t_{1/2}$ values of our AdipoR1Δ88 and AdipoR2Δ99 proteins are 74 and 20 min, respectively. The CPM profile of AdipoR2Δ99 revealed two phases, fast and slow, probably corresponding to the exposed and transmembrane cysteine residues, respectively, among which the latter reflect the stability of the transmembrane structure. In fact, AdipoR2Δ99 has more exposed cysteine residues than AdipoR1Δ88. Therefore, the $t_{1/2}$ value of 20 min for AdipoR2Δ99 may be an underestimate. Consequently, we concluded that both of the present preparations of AdipoR1Δ88 and AdipoR2Δ99 are sufficiently stable. Second, the lipids that co-purified with the AdipoR1Δ88 and AdipoR2Δ99 in these preparations were analyzed by TLC [32] (Fig. 4c–e). Several lipid species co-purified with AdipoR1Δ88 and AdipoR2Δ99, as well as the full-length proteins, indicating that the "bound lipids", which are important for the native folding of the membrane proteins, are probably retained in these preparations. Third, the purified AdipoR1Δ88 protein was reconstituted into liposomes by the reported method [33]. The reconstituted proteoliposomes exhibited the binding activity for osmotin (K_D = 0.7 μM; R_{max} = 49.2 RU) in the SPR analysis. Together, these results confirmed that we have successfully prepared structurally and functionally intact samples of AdipoR1 and AdipoR2 that are suitable for crystallization.

Thus, crystallization trials of AdipoR1Δ88 and AdipoR2Δ99 were performed with commercially available kits, such as MemStart, MemSys, and MemGold (Molecular Dimensions), by the vapor diffusion method. First, AdipoR2Δ99 crystals were obtained in one of the MemGold kit conditions. Despite extensive attempts to optimize the crystallization conditions to improve the crystal quality, no diffraction was obtained from these crystals. Furthermore, crystallization trials by the lipidic mesophase method were performed for the AdipoR1Δ88 and AdipoR2Δ99 preparations. However, crystals were obtained only in a limited number of conditions, and their diffractions were all poor (data not shown). Consequently, these results indicated that improvement of the crystal packing was necessary.

Antibody generation

Antibody fragments are useful tools to improve the resolution in membrane protein crystallography [34]. In fact, GPCRs, such as the β_2 adrenergic receptor and the A_{2A}

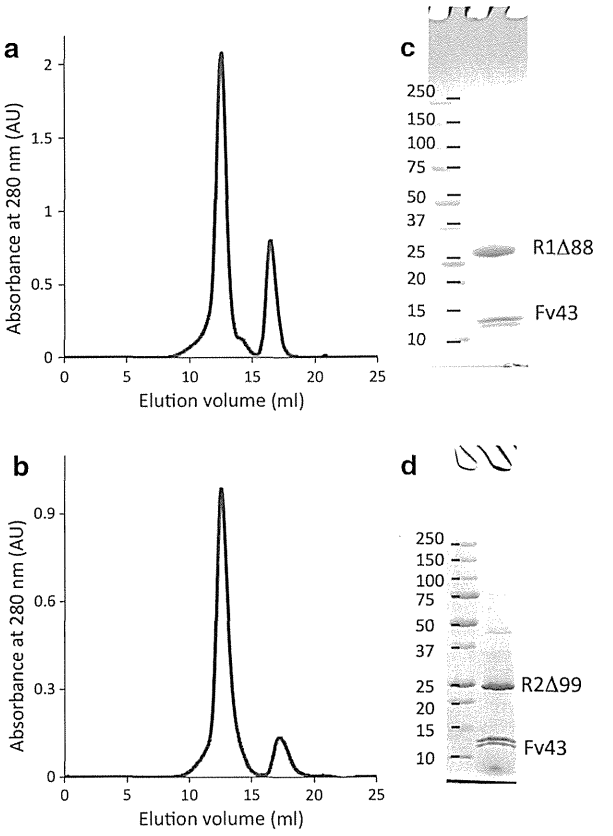

Fig. 6 Isolation of the AdipoR1Δ88·Fv43 and AdipoR2Δ99·Fv43 complexes. **a**, **b** Gel filtration chromatograms of the AdipoR1Δ88·Fv43 (**a**) and AdipoR2Δ99·Fv43 (**b**) complexes. **c**, **d** SDS-PAGE analysis of the crystallization samples of the AdipoR1Δ88·Fv43 (**c**) and AdipoR2Δ99·Fv43 (**d**) complexes

adenosine receptor, were co-crystallized with antibody fragments [35, 36]. Therefore, we planned to produce a high affinity and conformational epitope-recognizing anti-AdipoR1 antibody, to improve the crystal packing of AdipoR1. The purified untagged AdipoR1Δ88 was reconstituted into liposomes, and the resultant proteoliposomes were used as the immunogen. Mouse anti-AdipoR1 antibodies were produced by a conventional hybridoma system. Proteoliposomes containing the purified AdipoR1Δ88 and biotinyl-PE were used for screening the antibodies by ELISA (liposome-ELISA). In the first round of liposome-ELISA from 960 wells of hybridoma cultures, 72 positive wells were selected (Fig. 5a). Subsequently, 11 positive clones were selected in the second round of liposome-ELISA and FSEC (Fig. 5b). Finally, 2 stable hybridoma cell lines (clone #43 and clone #55) were established. The denatured dot blot analysis showed that IgG#43 recognized the native conformation of AdipoR1, whereas IgG#55 recognized the linear epitope (Fig. 5c). In addition, ELISA and FSEC analyses revealed that both IgG#43 and IgG#55 cross-reacted with AdipoR2Δ99 (data not shown). The cDNAs encoding the V_H and V_L regions of IgG#43 were cloned from hybridoma cells, according to the standard method [18]. The very N-terminal amino acid residues of the V_H and V_L fragments were determined by Edman degradation, and the 15 residue sequences of the N-termini of the V_H and V_L regions from clone #43 were determined as EVLLQQSGPELVKPG and DIQMTQSPASLSASV, respectively. The base sequences of the cloned cDNAs were corrected accordingly. The variable region of IgG#43 (Fv43) was synthesized by the *E. coli* cell-free protein synthesis method, and purified to homogeneity by column chromatography. The yield of the purified Fv43 was 0.3 mg per 1 ml cell-free synthesis reaction.

Data collection and processing

The cell-free produced Fv43 was mixed with the purified AdipoR1Δ88 and AdipoR2Δ99, and the AdipoR1Δ88·Fv43 and AdipoR2Δ99·Fv43 complexes were isolated by gel filtration chromatography (Fig. 6). The AdipoR1Δ88·Fv43 and AdipoR2Δ99·Fv43 complexes were crystallized by the lipidic mesophase method. The AdipoR1Δ88·Fv43 crystals with 10–15 μm lengths were obtained in 100 mM bicine buffer (pH 8.0) containing 50–150 mM $MgSO_4$ and 29–33 % (v/v) PEG400 (Fig. 7a, b). The AdipoR2Δ99·Fv43 crystals with 30–40 μm lengths were obtained in 100 mM Na-citrate buffer (pH 6.0) containing 375–425 mM K-citrate and 28–30 % (v/v) PEG400 (Fig. 7c, d). The crystals reached their full sizes within one week.

We successfully collected all of the data sets by the helical scan method, with a microbeam of 1 μm × 10 μm (horizontal × vertical) at beamline BL32XU at SPring-8 [24–26]. The AdipoR1Δ88·Fv43 and AdipoR2Δ99·Fv43 crystals diffracted up to 2.8 and 2.2 Å resolutions, respectively (Fig. 8). Data collection from the AdipoR1 crystal was limited to 10–30 images per crystal, due to radiation damage in the microcrystals, and therefore the data from six crystals were merged to complete the data set. The diffraction data of the AdipoR2 crystal were collected from a single crystal. The data collection statistics are shown in Table 1. The AdipoR1Δ88·Fv43 and AdipoR2Δ99·Fv43 crystals belonged to the space groups $C222_1$, with unit cell parameters $a = 92.7$, $b = 194.4$, $c = 74.4$ Å, and $P2_12_12$, with unit cell parameters $a = 74.6$, $b = 108.6$, $c = 101.0$ Å, respectively. Under the assumption that the asymmetric unit contained one AdipoR1Δ88·Fv43 complex or one AdipoR2Δ99·Fv43 complex, the Matthews coefficients of the AdipoR1Δ88·Fv43 and AdipoR2Δ99·Fv43 complexes were calculated to be 2.8 $Å^3\ Da^{-1}$ with a solvent content of 56.1 % and 3.6 $Å^3Da^{-1}$ with a solvent content of 65.4 %, respectively. An initial phase for the AdipoR2Δ99·Fv43 complex was obtained by molecular replacement using the Fv fragment (the V_H and V_L fragments from

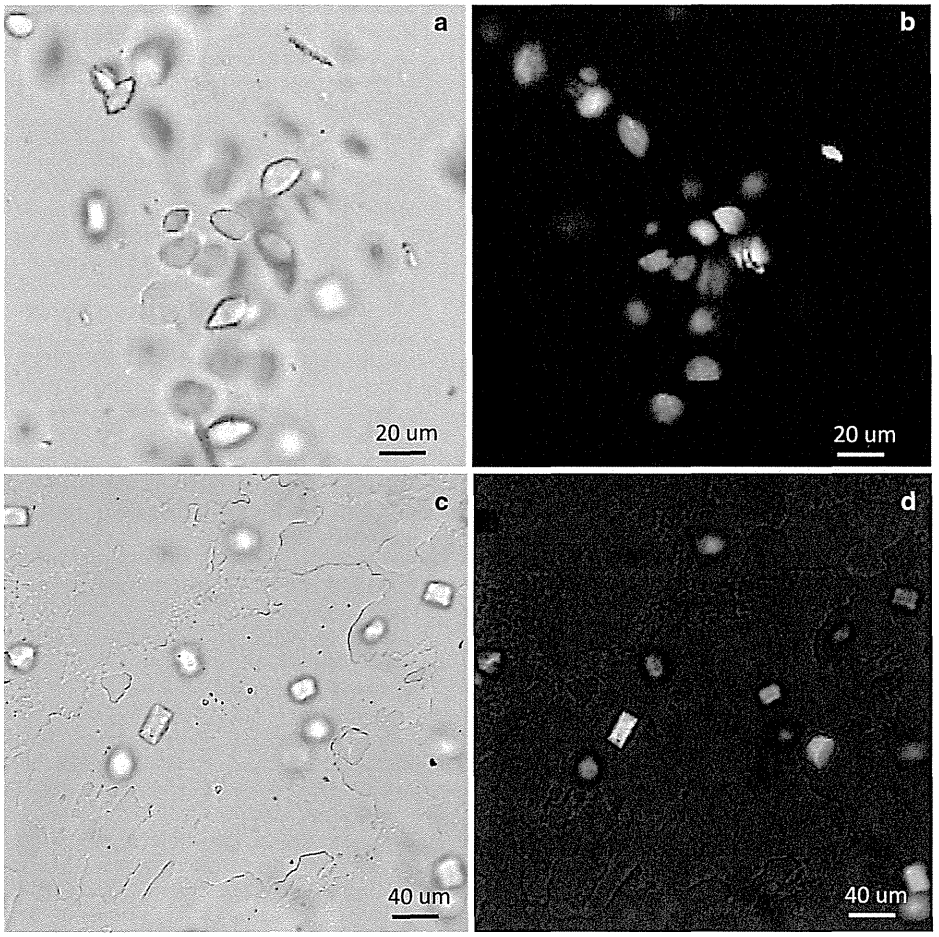

Fig. 7 Crystals of the FLAG-tagged AdipoR1Δ88·Fv43 and AdipoR2Δ99·Fv43 complexes. **a**, **b** Crystals of the FLAG-tagged AdipoR1Δ88·Fv43 complex. **c**, **d** Crystals of the AdipoR2Δ99·Fv43 complex. Crystals are shown in bright field (**a**, **c**) and under crossed polarizers (**b**, **d**)

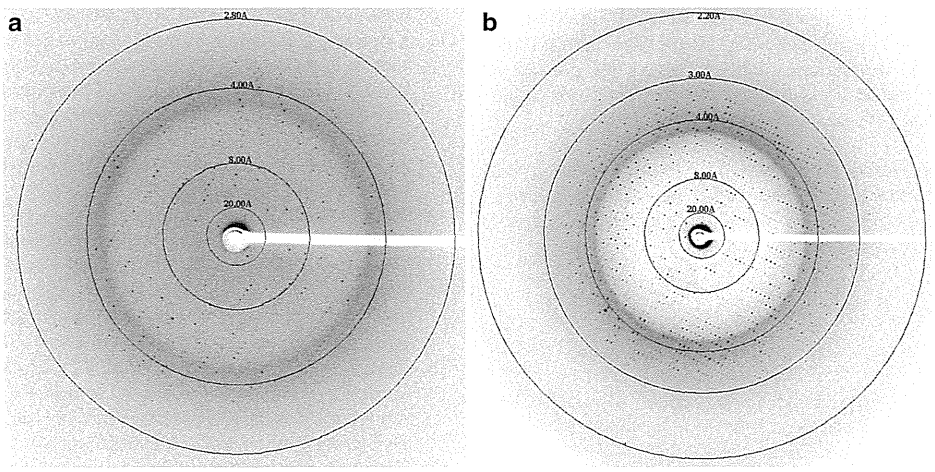

Fig. 8 X-ray diffraction images of the AdipoR1Δ88·Fv43 complex (**a**) and the AdipoR2Δ99·Fv43 complex (**b**)

Table 1 Data collection statistics

Structure	AdipoR1Δ88·Fv43 complex	AdipoR2Δ99·Fv43 complex
No. of crystals	6	1
X-ray source	BL32XU, SPring-8	BL32XU, SPring-8
Wavelength (Å)	1	1
Space group	$C222_1$	$P2_12_12$
Cell dimensions		
a, *b*, *c* (Å)	92.7, 194.4, 74.4	74.6, 108.6, 101.0
α, β, γ (°)	90.0, 90.0, 90.0	90.0, 90.0, 90.0
No. of reflections measured	135111	145165
No. of unique reflections	16509	32174
Resolution (Å)	20.00–2.80 (2.90–2.80)	19.52–2.40 (2.49–2.40)
R_{merge}	0.176 (>1)	0.115 (1.297)
Mean $I/\sigma(I)$	8.5 (1.3)	8.6 (1.2)
Completeness (%)	97.2 (99.1)	98.3 (99.4)
Redundancy	8.2 (8.0)	4.5 (4.5)
V_M ($Å^3$ Da^{-1})	2.8	3.6
Solvent content (%)	56.1	65.4

Values in parentheses are for the outer shell

PDB IDs 1E6J and 1FDL, respectively) in Phaser [37] as search models. The refinement is in progress.

Acknowledgments This work was supported by grants from the Targeted Proteins Research Program (S.Y., T.K., S.I., and M.Y.) and the Platform for Drug Discovery, Informatics, and Structural Life Science (S.Y. and M.Y.) from the Ministry of Education, Culture, Sports, Science and Technology of Japan, and by the research acceleration program of the Japan Science and Technology Agency (S.I.). We thank M. Toyama, M. Inoue, M. Goto, M. Aoki, and K. Ishii for expression plasmid preparation, M. Nishimoto, Y. Tomabechi, and Y. Terazawa for technical assistance with protein expression and purification, and R. Akasaka for protein analysis. The synchrotron radiation experiments were performed on BL32XU at SPring-8 (Proposal Nos. 2012A1332, 2012B1453, 2013B1034, 2014A1008, and 2014A1186) with the approval of RIKEN. We are also grateful to the staffs of I24 (Diamond Light Source) and X06SA (Swiss Light Source) for assistance with data collection.

References

1. Scherer PE, Williams S, Fogliano M, Baldini G, Lodish HF (1995) A novel serum protein similar to C1q, produced exclusively in adipocytes. J Biol Chem 270(45):26746–26749
2. Hu E, Liang P, Spiegelman BM (1996) AdipoQ is a novel adipose-specific gene dysregulated in obesity. J Biol Chem 271 (18):10697–10703
3. Maeda K, Okubo K, Shimomura I, Funahashi T, Matsuzawa Y, Matsubara K (1996) cDNA cloning and expression of a novel adipose specific collagen-like factor, apM1 (AdiPose Most abundant Gene transcript 1). Biochem Biophys Res Commun 221(2):286–289
4. Nakano Y, Tobe T, Choi-Miura NH, Mazda T, Tomita M (1996) Isolation and characterization of GBP28, a novel gelatin-binding protein purified from human plasma. J Biochem 120(4):803–812
5. Hotta K, Funahashi T, Arita Y, Takahashi M, Matsuda M, Okamoto Y, Iwahashi H, Kuriyama H, Ouchi N, Maeda K, Nishida M, Kihara S, Sakai N, Nakajima T, Hasegawa K, Muraguchi M, Ohmoto Y, Nakamura T, Yamashita S, Hanafusa T, Matsuzawa Y (2000) Plasma concentrations of a novel, adipose-specific protein, adiponectin, in type 2 diabetic patients. Arterioscler Thromb Vasc Biol 20(6):1595–1599
6. Yamauchi T, Kamon J, Ito Y, Tsuchida A, Yokomizo T, Kita S, Sugiyama T, Miyagishi M, Hara K, Tsunoda M, Murakami K, Ohteki T, Uchida S, Takekawa S, Waki H, Tsuno NH, Shibata Y, Terauchi Y, Froguel P, Tobe K, Koyasu S, Taira K, Kitamura T, Shimizu T, Nagai R, Kadowaki T (2003) Cloning of adiponectin receptors that mediate antidiabetic metabolic effects. Nature 423(6941):762–769
7. Tomas E, Tsao TS, Saha AK, Murrey HE, Zhang CC, Itani SI, Lodish HF, Ruderman NB (2002) Enhanced muscle fat oxidation and glucose transport by ACRP30 globular domain: acetyl-CoA carboxylase inhibition and AMP-activated protein kinase activation. Proc Natl Acad Sci USA 99(25):16309–16313
8. Yamauchi T, Kamon J, Minokoshi Y, Ito Y, Waki H, Uchida S, Yamashita S, Noda M, Kita S, Ueki K, Eto K, Akanuma Y, Froguel P, Foufelle F, Ferre P, Carling D, Kimura S, Nagai R, Kahn BB, Kadowaki T (2002) Adiponectin stimulates glucose utilization and fatty-acid oxidation by activating AMP-activated protein kinase. Nat Med 8(11):1288–1295
9. Kahn BB, Alquier T, Carling D, Hardie DG (2005) AMP-activated protein kinase: ancient energy gauge provides clues to modern understanding of metabolism. Cell Metab 1(1):15–25
10. Iwabu M, Yamauchi T, Okada-Iwabu M, Sato K, Nakagawa T, Funata M, Yamaguchi M, Namiki S, Nakayama R, Tabata M, Ogata H, Kubota N, Takamoto I, Hayashi YK, Yamauchi N, Waki H, Fukayama M, Nishino I, Tokuyama K, Ueki K, Oike Y, Ishii S, Hirose K, Shimizu T, Touhara K, Kadowaki T (2010) Adiponectin and AdipoR1 regulate PGC-1α and mitochondria by Ca^{2+} and AMPK/SIRT1. Nature 464(7293):1313–1319
11. Kersten S, Desvergne B, Wahli W (2000) Roles of PPARs in health and disease. Nature 405(6785):421–424
12. Yamauchi T, Kamon J, Waki H, Imai Y, Shimozawa N, Hioki K, Uchida S, Ito Y, Takakuwa K, Matsui J, Takata M, Eto K, Terauchi Y, Komeda K, Tsunoda M, Murakami K, Ohnishi Y, Naitoh T, Yamamura K, Ueyama Y, Froguel P, Kimura S, Nagai R, Kadowaki T (2003) Globular adiponectin protected ob/ob mice from diabetes and ApoE-deficient mice from atherosclerosis. J Biol Chem 278(4):2461–2468
13. Wess J (1997) G-protein-coupled receptors: molecular mechanisms involved in receptor activation and selectivity of G-protein recognition. FASEB J 11(5):346–354
14. Alexandrov AI, Mileni M, Chien EY, Hanson MA, Stevens RC (2008) Microscale fluorescent thermal stability assay for membrane proteins. Structure 16(3):351–359
15. Hanson MA, Cherezov V, Griffith MT, Roth CB, Jaakola VP, Chien EY, Velasquez J, Kuhn P, Stevens RC (2008) A specific cholesterol binding site is established by the 2.8 Å structure of the human β_2-adrenergic receptor. Structure 16(6):897–905
16. Kohler G, Milstein C (1975) Continuous cultures of fused cells secreting antibody of predefined specificity. Nature 256(5517): 495–497

17. Hino T, Iwata S, Murata T (2013) Generation of functional antibodies for mammalian membrane protein crystallography. Curr Opin Struct Biol 23(4):563–568
18. Toleikis L, Broders O, Dubel S (2004) Cloning single-chain antibody fragments (scFv) from hybridoma cells. Methods Mol Med 94:447–458
19. Yabuki T, Motoda Y, Hanada K, Nunokawa E, Saito M, Seki E, Inoue M, Kigawa T, Yokoyama S (2007) A robust two-step PCR method of template DNA production for high-throughput cell-free protein synthesis. J Struct Funct Genomics 8(4):173–191
20. Kigawa T, Yabuki T, Matsuda N, Matsuda T, Nakajima R, Tanaka A, Yokoyama S (2004) Preparation of *Escherichia coli* cell extract for highly productive cell-free protein expression. J Struct Funct Genomics 5(1–2):63–68
21. Matsuda T, Watanabe S, Kigawa T (2013) Cell-free synthesis system suitable for disulfide-containing proteins. Biochem Biophys Res Commun 431(2):296–301
22. Hato M, Yamashita J, Shiono M (2009) Aqueous phase behavior of lipids with isoprenoid type hydrophobic chains. J Phys Chem B 113(30):10196–10209
23. Hato M, Hosaka T, Tanabe H, Kitsunai T, Yokoyama S (2014) A new manual dispensing system for in meso membrane protein crystallization with using a stepping motor-based dispenser. J Struct Funct Genomics 15(3):165–171
24. Ueno G, Kanda H, Kumasaka T, Yamamoto M (2005) Beamline Scheduling Software: administration software for automatic operation of the RIKEN structural genomics beamlines at SPring-8. J Synchrotron Radiat 12(Pt 3):380–384
25. Murakami I, Fujii T, Kameyama K, Iwata T, Saito M, Kubushiro K, Aoki D (2012) Tumor volume and lymphovascular space invasion as a prognostic factor in early invasive adenocarcinoma of the cervix. J Gynecol Oncol 23(3):153–158
26. Hirata K, Kawano Y, Ueno G, Hashimoto K, Murakami H, Hasegawa K, Hikima T, Kumasaka T, Yamamoto M (2013) Achievement of protein micro-crystallography at SPring-8 beamline BL32XU. J Phys Conf Ser 425:012002
27. Otwinowski Z, Minor W (1997) Processing of X-ray diffraction data collected in oscillation mode. Methods Enzymol 276:307–327
28. Kabsch W (2010) Xds. Acta Crystallogr D Biol Crystallogr 66(Pt 2):125–132
29. Buchan DW, Minneci F, Nugent TC, Bryson K, Jones DT (2013) Scalable web services for the PSIPRED protein analysis workbench. Nucleic Acids Res 41(Web Server issue):W349–W357
30. Tusnady GE, Simon I (2001) The HMMTOP transmembrane topology prediction server. Bioinformatics 17(9):849–850
31. Sonoda Y, Newstead S, Hu NJ, Alguel Y, Nji E, Beis K, Yashiro S, Lee C, Leung J, Cameron AD, Byrne B, Iwata S, Drew D (2011) Benchmarking membrane protein detergent stability for improving throughput of high-resolution X-ray structures. Structure 19(1):17–25
32. Han X, Cheng H (2005) Characterization and direct quantitation of cerebroside molecular species from lipid extracts by shotgun lipidomics. J Lipid Res 46(1):163–175
33. Rigaud JL, Levy D (2003) Reconstitution of membrane proteins into liposomes. Methods Enzymol 372:65–86
34. Iwata S, Ostermeier C, Ludwig B, Michel H (1995) Structure at 2.8 Å resolution of cytochrome *c* oxidase from *Paracoccus denitrificans*. Nature 376(6542):660–669
35. Rasmussen SG, DeVree BT, Zou Y, Kruse AC, Chung KY, Kobilka TS, Thian FS, Chae PS, Pardon E, Calinski D, Mathiesen JM, Shah ST, Lyons JA, Caffrey M, Gellman SH, Steyaert J, Skiniotis G, Weis WI, Sunahara RK, Kobilka BK (2011) Crystal structure of the β_2 adrenergic receptor-Gs protein complex. Nature 477(7366):549–555
36. Hino T, Arakawa T, Iwanari H, Yurugi-Kobayashi T, Ikeda-Suno C, Nakada-Nakura Y, Kusano-Arai O, Weyand S, Shimamura T, Nomura N, Cameron AD, Kobayashi T, Hamakubo T, Iwata S, Murata T (2012) G-protein-coupled receptor inactivation by an allosteric inverse-agonist antibody. Nature 482(7384):237–240
37. McCoy AJ, Grosse-Kunstleve RW, Adams PD, Winn MD, Storoni LC, Read RJ (2007) Phaser crystallographic software. J Appl Crystallogr 40(Pt 4):658–674
38. Larkin MA, Blackshields G, Brown NP, Chenna R, McGettigan PA, McWilliam H, Valentin F, Wallace IM, Wilm A, Lopez R, Thompson JD, Gibson TJ, Higgins DG (2007) Clustal W and Clustal X version 2.0. Bioinformatics 23(21):2947–2948

nature COMMUNICATIONS

ARTICLE

Received 9 Dec 2013 | Accepted 8 Jan 2015 | Published 26 Feb 2015

DOI: 10.1038/ncomms7241 OPEN

Complement C1q-induced activation of β-catenin signalling causes hypertensive arterial remodelling

Tomokazu Sumida[1,2], Atsuhiko T. Naito[1,2,3], Seitaro Nomura[1], Akito Nakagawa[3], Tomoaki Higo[3], Akihito Hashimoto[3], Katsuki Okada[3], Taku Sakai[3], Masamichi Ito[1], Toshihiro Yamaguchi[1], Toru Oka[2,3], Hiroshi Akazawa[1,2], Jong-Kook Lee[2,3], Tohru Minamino[4], Stefan Offermanns[5], Tetsuo Noda[6], Marina Botto[7], Yoshio Kobayashi[8], Hiroyuki Morita[1], Ichiro Manabe[1], Toshio Nagai[8], Ichiro Shiojima[2,9] & Issei Komuro[1,2,3]

Hypertension induces structural remodelling of arteries, which leads to arteriosclerosis and end-organ damage. Hyperplasia of vascular smooth muscle cells (VSMCs) and infiltration of immune cells are the hallmark of hypertensive arterial remodelling. However, the precise molecular mechanisms of arterial remodelling remain elusive. We have recently reported that complement C1q activates β-catenin signalling independent of Wnts. Here, we show a critical role of complement C1-induced activation of β-catenin signalling in hypertensive arterial remodelling. Activation of β-catenin and proliferation of VSMCs were observed after blood-pressure elevation, which were prevented by genetic and chemical inhibition of β-catenin signalling. Macrophage depletion and *C1qa* gene deletion attenuated the hypertension-induced β-catenin signalling, proliferation of VSMCs and pathological arterial remodelling. Our findings unveil the link between complement C1 and arterial remodelling and suggest that C1-induced activation of β-catenin signalling becomes a novel therapeutic target to prevent arteriosclerosis in patients with hypertension.

[1] Department of Cardiovascular Medicine, The University of Tokyo Graduate School of Medicine, Tokyo 113-8655, Japan. [2] CREST, Japan Science and Technology Agency, Tokyo 102-0075, Japan. [3] Department of Cardiovascular Medicine, Osaka University Graduate School of Medicine, Osaka 565-0871, Japan. [4] Department of Cardiovascular Biology and Medicine, Niigata University Graduate School of Medical and Dental Sciences, Niigata 951-8510, Japan. [5] Department of Pharmacology, Max-Planck-Institute for Heart and Lung Research, Bad Nauheim D-61231, Germany. [6] Department of Cell Biology, The Cancer Institute, Japanese Foundation for Cancer Research, Tokyo 135-8550, Japan. [7] Centre for Complement and Inflammation Research, Department of Medicine, Imperial College London, London SW7 2AZ, UK. [8] Department of Cardiovascular Medicine, Chiba University Graduate School of Medicine, Chiba 260-8670, Japan. [9] Department of Medicine II, Kansai Medical University, Osaka 573-1191, Japan. Correspondence and requests for materials should be addressed to I.K. (email: komuro-tky@umin.ac.jp).

Hypertension, as the leading risk factor for various cardiovascular diseases, caused 9.4 million deaths in 2010 (ref. 1). In 2000, nearly one billion people have hypertension worldwide, and that number is estimated to increase to 1.5 billion by 2025 (ref. 2). One direct physiological consequence of blood-pressure elevation is the structural remodelling of the arteries. Prolonged high blood pressure causes arterial degeneration due to lack of capability of optimized remodelling, leading to pathological conditions such as arteriosclerosis and end-organ damage[3,4]. Hypertrophy/hyperplasia of vascular smooth muscle cells (VSMCs) and infiltration of inflammatory cells are the characteristics of pathological arterial remodelling[4–6]. A variety of humoral factors such as growth factors, proteases and cytokines, secreted by infiltrated immune cells, have been reported to be involved in VSMC proliferation[3,7], however, precise molecular and cellular mechanisms of how hypertensive arterial remodelling is developed remain elusive.

Wnt/β-catenin signalling is an evolutionarily conserved intracellular signalling that plays an important role in embryonic development and various diseases[7,8]. The Wnt/β-catenin pathway is the most well-understood signalling cascade initiated by Wnt proteins and acts as a mitogenic signal during the development of multiple organs, and the aberrant activation of Wnt/β-catenin signalling pathway is often associated with cancer[9–11]. Wnt/β-catenin signalling regulates the proliferation and differentiation of smooth muscle cells during embryonic and postnatal angiogenesis[12,13]. Furthermore, activation of Wnt/β-catenin signalling is implicated in VSMC proliferation during intimal thickening after vascular injury[14,15].

Recently, we have reported that complement protein C1q, an initiator of the classical complement pathway, activates canonical Wnt signalling in a complement cascade-independent manner[16]. Given that the major source of complement C1q is monocyte-derived cells[17] and that macrophages (Mϕs) within the aortic wall play a vital role in pathogenesis of arterial remodelling, we hypothesized that aortic Mϕ-derived C1q activates β-catenin signalling and induces proliferation of VSMCs. In the present study, we elucidated that complement C1q, which is mainly secreted by alternatively activated aortic Mϕs, is involved in hypertensive arterial remodelling via activation of β-catenin signalling.

Results

VSMC proliferation as an early event in hypertension. Infusion of angiotensin II (AngII) (1.8 μg kg^{-1} min^{-1}) to male C57BL/6 mice increased blood pressure by ~70 mm Hg and promoted arterial remodelling characterized by thickening and dilation of the abdominal aorta at 6 weeks after AngII infusion (Fig. 1a–c), as reported previously[18]. The number of 5-bromo-2′deoxyuridine (BrdU)-positive, proliferating VSMCs was significantly increased as early as 1 week after AngII infusion (Fig. 1d), when the gross structural remodelling of the arteries was not observed. These results suggest that VSMC proliferation is one of the earliest events that occur in response to AngII-induced blood-pressure elevation.

β-catenin signalling is activated at early hypertension. Various growth factors and G-protein-coupled receptor agonists induce VSMC proliferation[7,19], and their mitogenic effects are often given by the activation of the mitogen-activated protein kinases, especially the extracellular signal regulated kinase (ERK) signalling pathway[5,20]. Therefore, we first examined whether ERK signalling was activated concurrently with VSMC proliferation after AngII infusion, and found that there was no increase in the phosphorylation levels of ERK1/2 (Supplementary Fig. 1a). Moreover, AngII activated ERK1/2 but had no effect on proliferation of cultured human aortic smooth muscle cells (HASMCs) (Supplementary Fig. 1b,c), suggesting that signalling pathways other than the ERK pathway play a key role in VSMC proliferation at the early stage of AngII-induced hypertension.

Wnt/β-catenin signalling has been reported to regulate proliferation and differentiation of smooth muscle cells during embryonic and postnatal angiogenesis[12,13] and intimal thickening after vascular injury[14,15]. We therefore tested whether β-catenin signalling was involved in VSMC proliferation after AngII infusion. Activation of β-catenin signalling upregulates the expression of Wnt/β-catenin target genes including *Axin2*

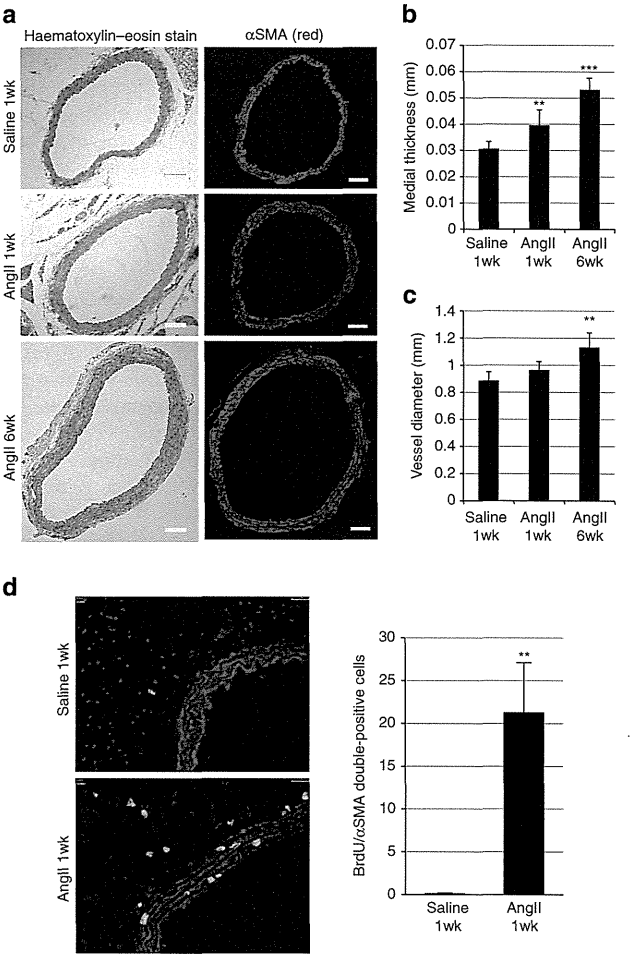

Figure 1 | Proliferation of VSMCs is observed at the initial stage of AngII-induced arterial remodelling. (**a**) Haematoxylin and eosin staining and immunostaining for α-smooth muscle actin (αSMA) of the abdominal aorta from 1-week saline-infused mice (saline 1wk), 1-week AngII-infused mice (AngII 1wk) and 6-week AngII-infused mice (AngII 6wk) ($n=5$–7). Scale bar, 100 μm. (**b**,**c**) Morphometric analysis. (**b**) Medial thickness and (**c**) vessel diameter were calculated using ImageJ. $^{**}P<0.01$, $^{***}P<0.001$ versus saline-infused mice ($n=5$–9). (**d**) Aortic tissues were immunostained for BrdU (green) and αSMA (red). Scale bar, 100 μm. The number of double-positive (BrdU(+)/αSMA(+)) cells per section is shown. $^{**}P<0.01$ versus saline-infused mice ($n=5$–7). Statistical significance was determined using one-way analysis of variance with Turkey's *post hoc* test for **b** and **c**, and the unpaired two-tailed Student's *t*-test for **d**. Results are represented as mean ± s.d.

(ref. 10). At 1 week after AngII infusion, the number of LacZ-positive VSMCs was increased in Wnt reporter Axin2^{LacZ} mice[11] (Fig. 2a) and the aortic VSMCs were strongly stained for β-catenin and Axin2 in wild-type mice (Fig. 2b; Supplementary Fig. 2a,b). Western blot (WB) analysis revealed that the amount of non-phosphorylated, active β-catenin (ABC)[21] was increased (Fig. 2c), and gene expression analysis also showed upregulation of Wnt/β-catenin target genes in aortic tissue (Fig. 2d). Although β-catenin was also expressed in endothelial cells of aorta (Supplementary Fig. 2c), Axin2 expression was not induced in endothelial cells 1 week after AngII infusion (Fig. 2a,b; Supplementary Fig. 2b), suggesting that β-catenin signalling was more potently activated in aortic VSMCs rather than endothelial cells at the early stage of hypertension. Both activation of β-catenin signalling and proliferation of VSMCs were attenuated when we normalized blood pressure in AngII-infused mice by oral administration of hydralazine (Supplementary Fig. 3a–c). Taken together, these results suggested that the elevation of blood pressure was responsible in part for activation of β-catenin signalling in the aortic VSMCs during hypertensive arterial remodelling.

β-catenin signal activation induces VSMC proliferation. To determine whether the activation of β-catenin signalling induces proliferation of VSMCs, we first treated cultured HASMCs with Wnt3A, a canonical Wnt ligand, or lithium chloride, which stabilizes β-catenin by inhibiting glycogen synthase kinase-3. Both Wnt3A and lithium chloride treatment activated β-catenin signalling and induced proliferation of HASMCs (Fig. 3a,b). Moreover, overexpression of constitutively ABC also induced proliferation of HASMCs (Fig. 3c), suggesting that activation of β-catenin signalling is sufficient to induce VSMC proliferation *in vitro*. On the other hand, AngII treatment did not induce activation of β-catenin signalling or proliferation of HASMCs (Supplementary Figs 1c and 3d), but induced cellular hypertrophy of HASMCs (Supplementary Fig. 3e). We next examined whether activation of β-catenin signalling was required for AngII-induced VSMC proliferation *in vivo*. Intraperitoneal injection of PKF115-584, a small-molecule inhibitor of β-catenin signalling[22], suppressed VSMC proliferation without lowering blood pressure at 1 week after AngII infusion (Fig. 3d; Supplementary Fig. 3f). To further determine the role of the β-catenin signal in VSMCs, we generated smooth muscle cell-specific, tamoxifen-inducible, β-catenin knockout mice by crossing SMMHC-CreER^{T2} mice[23] with *Ctnnb1*$^{flox/flox}$ mice (SMMHC/β-catenin CKO). The expression levels of β-catenin and Axin2 in aortic tissue were downregulated when they were treated with tamoxifen (Fig. 4a–c). There was no change in systolic blood pressure of SMMHC/β-catenin CKO mice as compared with control mice (Fig. 4d). TdT-mediated dUTP nick end labelling staining revealed that there was no change in cell death and cell density in aortic media after tamoxifen treatment (Fig. 4e,f). There was less proliferation of VSMCs after AngII infusion in SMMHC/β-catenin CKO mice as compared with control mice (Fig. 4g), suggesting that activation of β-catenin signalling substantially contributes to enhanced proliferation of VSMCs at the early phase of hypertensive arterial remodelling.

Recruitment of Mϕs is essential for β-catenin signalling. Mϕs were recruited to the aortic adventitia by 1 week after AngII

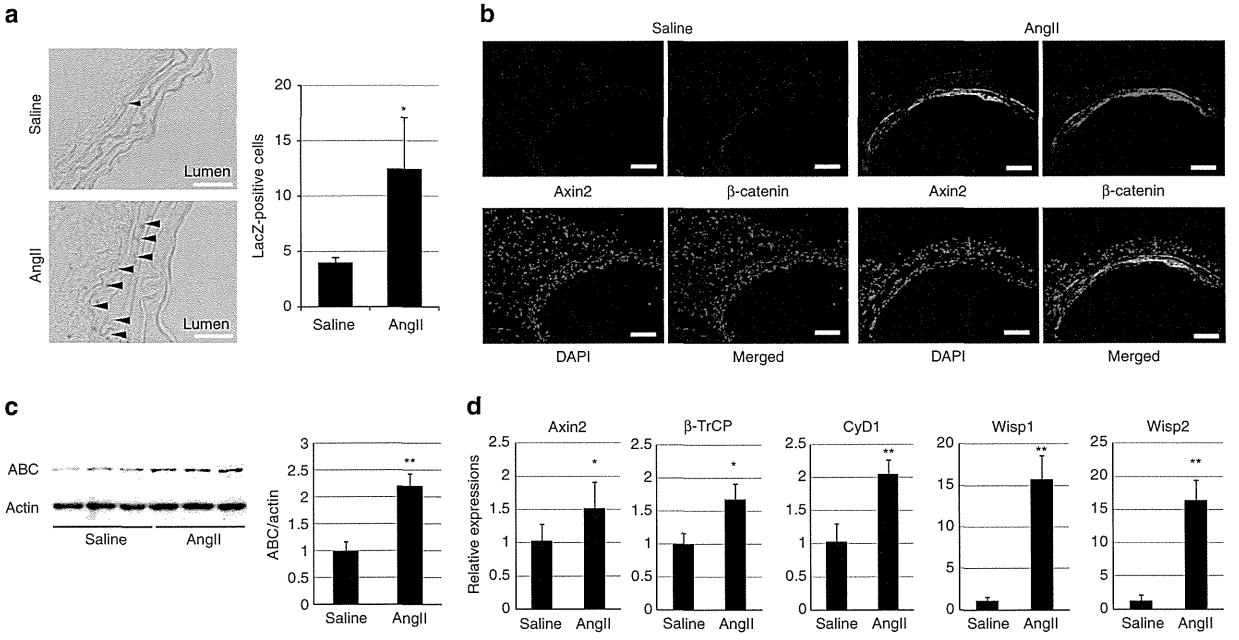

Figure 2 | β-catenin signalling is activated in the aortic media at the early stage of hypertension. (**a**) β-galactosidase staining of the aortic tissue from 1-week saline- or AngII-infused Axin2^{LacZ} mice. Arrowheads indicate β-galactosidase-positive nuclei. Scale bar, 50 μm. The number of LacZ-positive cells in the aortic media from Axin2^{LacZ} mice is shown. *$P<0.05$ versus saline-infused mice ($n=5$). (**b**) Aortic tissues from 1-week saline- or AngII-infused mice were immunostained for Axin2 (green) and β-catenin (red). Scale bar, 100 μm. (**c**) Western blot analysis for non-phosphorylated active β-catenin (ABC) in the aortic tissues from 1-week saline- or AngII-infused mice. Activation of β-catenin signalling was quantified by measuring the relative level of ABC over actin. The values are shown as fold induction over saline-infused mice. **$P<0.01$ versus saline-infused mice ($n=6$, 7). (**d**) Real-time PCR analysis for the expression levels of the β-catenin target genes (*Axin2, β-TrCP, cyclin D1 (CyD1), Wisp1* and *Wisp2*) in the aortic tissue from 1-week saline- or AngII-infused mice. The values are shown as fold induction over saline-infused mice. *$P<0.05$, **$P<0.01$ versus saline ($n=6$). Statistical significance was determined using the unpaired two-tailed Mann–Whitney *U*-test for **a**, **c** and **d**. Results are represented as mean ± s.d. DAPI, 4′,6-diamidino-2-phenylindole.

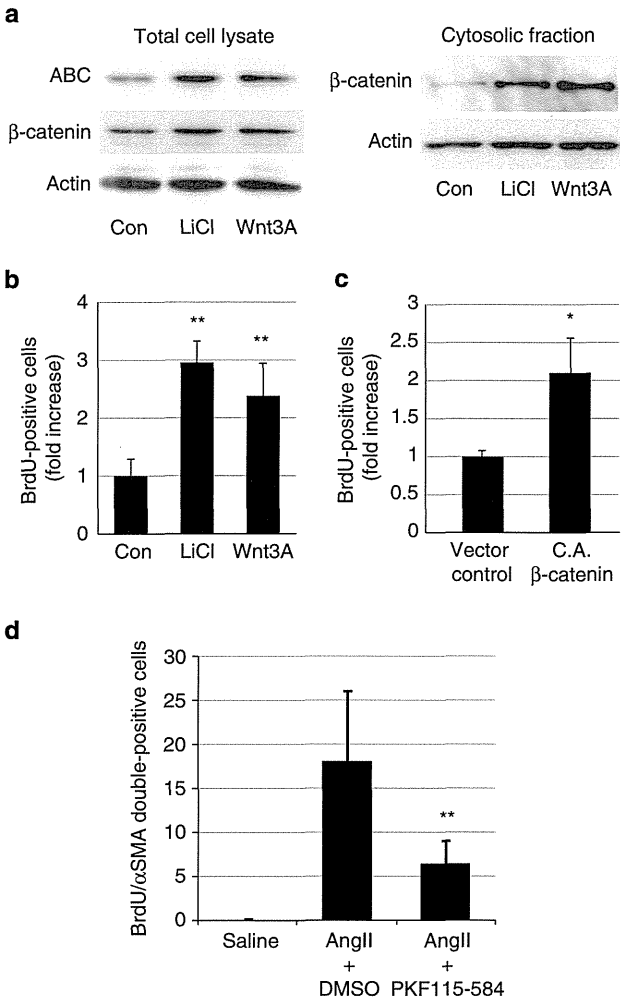

Figure 3 | Activation of β-catenin signalling induces VSMC proliferation. (**a**) Western blot analysis. HASMCs were treated with LiCl (10 mM) or Wnt3A (80 ng ml^{-1}), and the amount of ABC and cytosolic β-catenin was analysed. Activation of β-catenin signalling was quantified by measuring the relative level of ABC over actin. (**b**) The number of BrdU(+) HASMCs after LiCl (10 mM) or Wnt3A (80 ng ml^{-1}) treatment. The values are shown as fold induction over non-treated HASMCs (Con). $^{**}P<0.01$ versus non-treated HASMCs ($n=4$). (**c**) The number of BrdU(+) HASMCs after infection with control retrovirus (vector control) or with constitutively active β-catenin (CA β-catenin) whose phosphorylation sites at the N terminus are all mutated. The values are shown as fold induction over control vector-transfected HASMCs. $^{*}P<0.05$ versus control vector-transfected HASMCs ($n=3$). (**d**) The number of double-positive (BrdU(+)/αSMA(+)) cells per aortic section from saline-infused mice, AngII-infused mice treated with DMSO (solvent), and AngII-infused mice treated with PKF115-584. $^{**}P<0.01$ versus AngII-infused mice treated with DMSO ($n=8$). Statistical significance was determined using one-way analysis of variance with Turkey's *post hoc* test for **b**, the unpaired two-tailed Student's *t*-test for **c** and the Kruskal–Wallis test with Dunn's correction for multiple comparisons for **d**. Results are represented as mean ± s.d.

infusion (Fig. 5a; Supplementary Fig. 4a). To elucidate the role of these Mϕs, we injected liposomes containing clodronate (Clo-Lip)[24] before AngII infusion to deplete the cells of monocyte lineage. Clo-Lip treatment reduced the number of infiltrating Mϕs (Fig. 5b; Supplementary Fig. 4a), and strongly suppressed activation of β-catenin signalling and proliferation of VSMCs at 1 week after AngII infusion (Fig. 5c–e). These results suggest that infiltrating Mϕs play critical roles in activation of β-catenin signalling and proliferation of VSMCs at the early phase of arterial remodelling.

M2 Mϕs secrete a potent activator of β-catenin signalling. Mϕs change their phenotypes in response to various environmental factors. Classically activated Mϕs or M1 Mϕs are induced by lipopolysaccharide (LPS), interferon-γ and tumour necrosis factor, and secrete pro-inflammatory cytokines to increase their killing ability. On the other hand, alternatively activated Mϕs or M2 Mϕs are induced by interleukin (IL)-4 and IL-13, and contribute to tissue remodelling and wound healing[25]. To determine the phenotype of Mϕs that accumulate into the aortic wall at the early stage of arterial remodelling, we used flow cytometric analysis to characterize M1-type Mϕ for Ly6c expression and M2-type Mϕ for CD206 expression[26]. Approximately 40% of the aortic Mϕs from AngII-infused mice expressed CD206 (CD11b + F4/80 + CD206 + Ly6c −: M2 type) and ∼10% of them expressed Ly6c (CD11b + F4/80 + CD206-Ly6c +: M1 type) (Fig. 6a; Supplementary Fig. 4b). Immunofluorescent analysis also showed large numbers of CD206-positive Mϕs in aortic adventitia (Fig. 6b). These results prompted us to postulate that M2-type Mϕs secrete humoral factors that activate β-catenin signalling and induce proliferation of VSMCs. To test this hypothesis, we first examined the effects of humoral factors secreted by M2 Mϕs on VSMCs. The M1 or M2 phenotype was elicited *in vitro* by treating Raw264.7 cells with LPS or IL-4, respectively. Conditioned media (CM) from Raw264.7 cells treated with PBS (Con Raw264.7 CM), LPS (LPS Raw264.7 CM) or IL-4 (IL-4 Raw264.7 CM) were added to HASMCs. IL-4 Raw264.7 CM activated β-catenin signalling and promoted cell proliferation in HASMCs more potently than Con Raw264.7 CM or LPS Raw264.7 CM (Fig. 6c,d). As Raw264.7 cells are known to be already activated, we performed the same experiments using bone marrow-derived Mϕs (BMDMs), and found that CM from IL-4-treated BMDMs (IL-4 BMDM CM) activated β-catenin signalling and induced proliferation of VSMCs more than CM from PBS-treated BMDMs (Con BMDM CM) or LPS-treated BMDMs (LPS BMDM CM) (Supplementary Fig. 4c,d). These results collectively suggest that M2 Mϕs, recruited to the vessel wall in response to blood-pressure elevation, secrete a substance that activates β-catenin signalling in VSMCs, thereby inducing VSMC proliferation in a paracrine manner. Expression levels of canonical Wnt ligands (Wnt1, 2, 2b,3, 3a, 7a, 7b, 8a, 8b, 10a and 10b), which could activate the β-catenin signalling pathway[10,27–29], were not upregulated in Raw264.7 cells or BMDMs by IL-4-induced M2 polarization (Supplementary Fig. 4e,f).

Complement C1q is a Mϕ-derived β-catenin signal activator. We have recently reported that complement protein C1q, an initiator of the classical complement pathway, activates β-catenin signalling and induces aging-associated impairment of skeletal muscle regeneration[16]. Given that monocyte/Mϕ lineage has been shown to be the major source of C1q biosynthesis[17] and tumour-associated Mϕs have been reported to produce complement C1q[30], we examined whether β-catenin signalling was activated in VSMCs by M2 Mϕ-derived C1q. *In vitro*, M2-polarized Raw264.7 Mϕs by IL-4 treatment markedly increased *C1qa* gene expression compared with PBS-treated or LPS-treated Raw264.7 Mϕs (Fig. 7a). To examine whether C1q is predominantly produced by M2 Mϕs rather than M0 or M1 Mϕs *in vivo*, we sorted M0-type (CD11b + F4/80 +

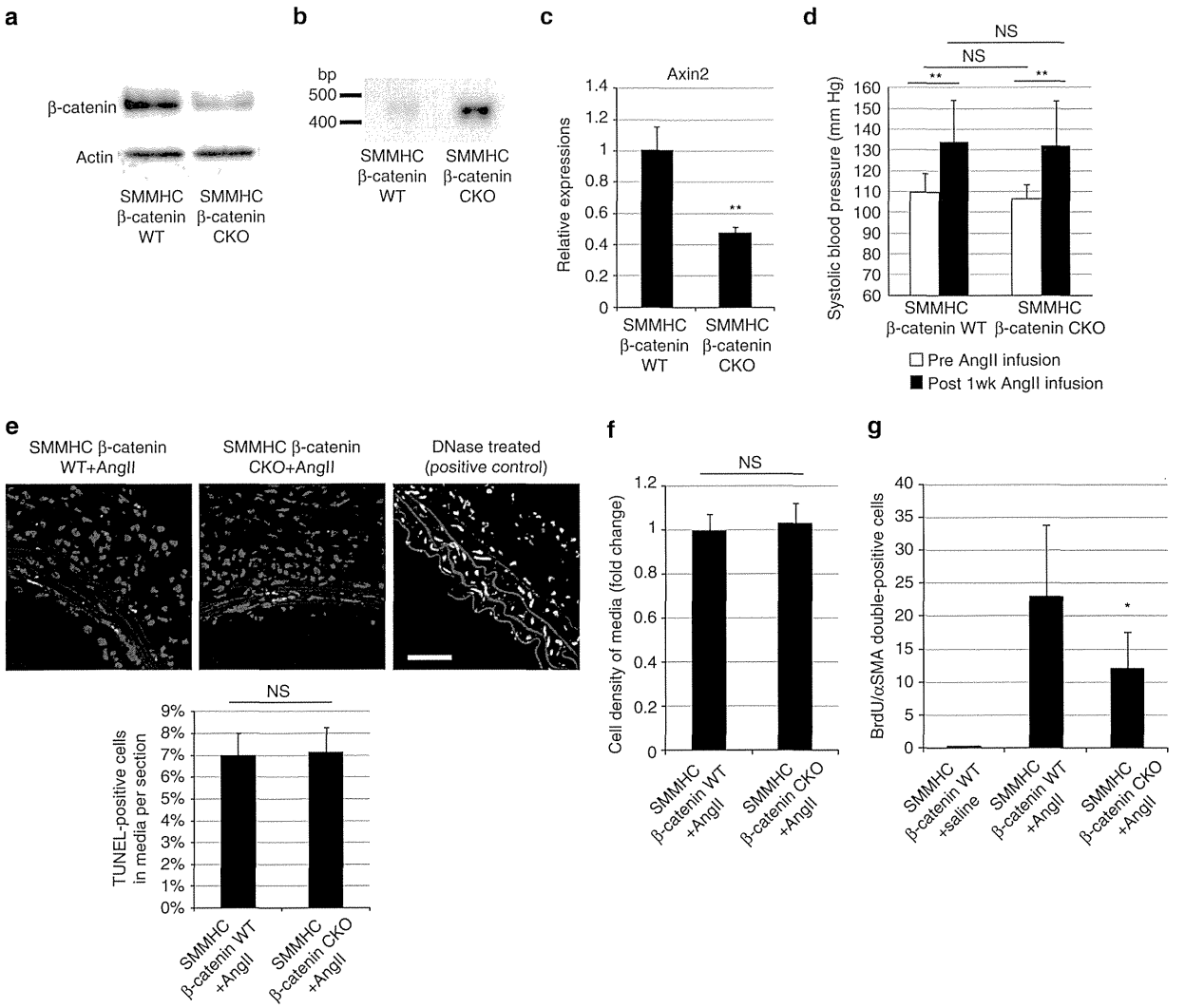

Figure 4 | β-catenin signal activation is responsible for VSMC proliferation after AngII infusion. (**a**) Western blot analysis. The amounts of β-catenin in the aortic tissues from SMMHC-CreER^{T2}:*Ctnnb1*$^{+/+}$ mice (SMMHC-β-catenin wild type (WT)) and SMMHC-CreER^{T2}:*Ctnnb1*$^{flox/flox}$ mice (SMMHC-β-catenin CKO) were analysed in aortic tissues isolated 6 days after the final tamoxifen treatment. (**b**) PCR analysis of aortic tissue DNA. DNA extracted from aortic tissues of tamoxifen-treated SMMHC-β-catenin WT and SMMHC-β-catenin CKO mice were amplified with a PCR primer set designed for detecting the null allele. (**c**) Real-time PCR analysis for the expression level of the *Axin2* gene (one of the major Wnt/β-catenin target genes) in the aortic tissue isolated from tamoxifen-treated SMMHC-β-catenin WT and SMMHC-β-catenin CKO mice. The values are shown as fold induction over SMMHC-β-catenin WT mice. $^{**}P<0.01$ versus SMMHC-β-catenin WT mice. (**d**) Systolic blood pressure before and after AngII infusion for 1 week. There was no difference in systolic blood pressure between SMMHC-β-catenin WT mice and SMMHC-β-catenin CKO mice before and after AngII infusion. $^{**}P<0.01$ versus Post 1wk AngII infusion. (**e**) TdT-mediated dUTP nick end labelling (TUNEL) staining of aortic tissue and percentage of TUNEL-positive cells. TUNEL staining of aortic tissue from SMMHC-β-catenin WT and SMMHC-β-catenin CKO mice 1 week after AngII infusion. The DNase (TACS nuclease)-treated section is presented as a positive control. Percentage of TUNEL-positive cells per total cells in aortic media was calculated. Scale bar, 50 μm. (**f**) Cell density of aortic media was calculated by measuring the number of αSMA-positive cells per field of view size ($40\times40\,\mu m^2$). (**g**) The number of double-positive (BrdU(+)/αSMA(+)) cells per aortic section from 1-week saline-infused SMMHC-CreER^{T2}:*Ctnnb1*$^{+/+}$ mice (SMMHC-β-catenin WT+saline), 1-week AngII-infused SMMHC-CreER^{T2}:*Ctnnb1*$^{+/+}$ mice (SMMHC-β-catenin WT+AngII) and SMMHC-CreER^{T2}:*Ctnnb1*$^{flox/flox}$ mice (SMMHC-β-catenin CKO+AngII). $^{*}P<0.05$ versus SMMHC-β-catenin WT+AngII ($n=12$). The values are shown as fold induction over SMMHC-β-catenin WT mice ($n=5$). Statistical significance was determined using the unpaired two-tailed Student's *t*-test for **c**, **e** and **f**, two-way analysis of variance followed by Sidak's multiple comparisons test for **d** and the Kruskal–Wallis test with Dunn's correction for multiple comparisons for **g**. Results are represented as mean ± s.d. NS, not significant.

CD206 − Ly6c −), M1-type (CD11b + F4/80 + CD206 − Ly6c +) and M2-type (CD11b + F4/80 + CD206 + Ly6c −) Mϕs from aortic tissue and compared the expression levels of C1q among three types of Mϕs, and found that M2-type Mϕs expressed more C1q than M0- or M1-type Mϕs (Fig. 7b; Supplementary Fig. 4b).

The direct effect of C1q on HASMCs was examined *in vitro*. C1q protein activated β-catenin signalling and promoted proliferation of cultured HASMCs in a dose-dependent manner, and these effects were suppressed by C1-inhibitor (C1-INH), an endogenous inhibitor of C1r and C1s (Fig. 7c,d; Supplementary Fig. 5a). Moreover, treatment with the C1

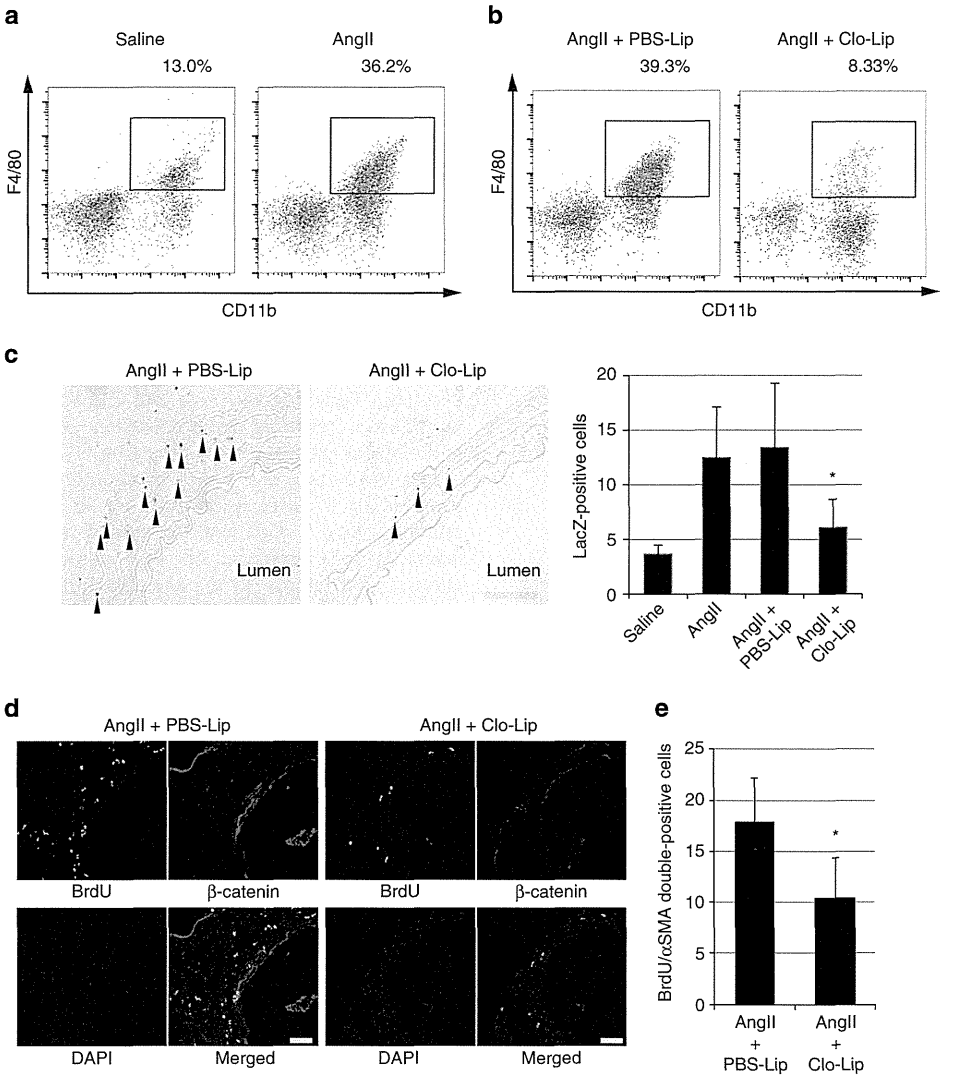

Figure 5 | Recruited Mϕs activate β-catenin signalling and induce VSMC proliferation after AngII infusion. (**a**,**b**) Representative density plots. Aortic Mϕs of 1-week saline- and AngII-infused mice (**a**) of and in AngII-infused mice treated with PBS liposome (PBS-Lip) or clodronate liposome (Clo-Lip) (**b**) were analysed by flow cytometry. Cells within the boxes are CD11b + F4/80 + Mϕs. The flow cytometric analysis was performed with pooled aortic tissues from a total of 3–10 mice and percent gated cell frequencies are indicated in each representative plot. (**c**) β-Galactosidase staining of the aortic tissue from AngII-infused $Axin2^{LacZ}$ mice, treated with PBS-Lip or Clo-Lip. Arrowheads indicate β-galactosidase-positive nuclei. Scale bar, 50 μm. The number of LacZ-positive cells in the media of aortic tissue from $Axin2^{LacZ}$ mice is shown. *$P<0.05$ versus PBS-Lip-treated AngII-infused mice ($n=5$–6). (**d**) Aortic tissues from AngII-infused mice treated with PBS-Lip or Clo-Lip were immunostained for BrdU (green) and β-catenin (red). Scale bar, 100 μm. (**e**) The number of double-positive (BrdU(+)/αSMA(+)) cells per aortic section from AngII-infused mice treated with PBS-Lip or Clo-Lip. *$P<0.05$ versus PBS-Lip-treated AngII-infused mice ($n=5$). Statistical significance was determined using one-way analysis of variance with Turkey's *post hoc* test for **c**, and the unpaired two-tailed Mann–Whitney *U*-test for **e**. Results are represented as mean ± s.d. DAPI, 4′,6-diamidino-2-phenylindole.

complex, which is composed of C1q, C1r and C1s, also activated β-catenin signalling in HASMCs, and this effect was inhibited by C1-INH (Supplementary Fig. 5b). WB analysis of cell culture media revealed that both C1r and C1s were secreted from HASMCs but not from Mϕs (Supplementary Fig. 5c,d). Activation of β-catenin signalling and proliferation of HASMCs induced by M2 Mϕ-CM was prevented by C1-INH (Fig. 7e,f; Supplementary Fig. 5e,f). These results collectively suggest that the C1 complex, which is composed of M2 Mϕ-derived C1q and VSMC-derived C1r/s is the factor that activates β-catenin signalling and induces proliferation of VSMCs.

C1-induced β-catenin signalling causes arterial remodelling. We next examined whether C1 is responsible for hypertension-induced activation of β-catenin signalling and proliferation of VSMCs *in vivo*. Expression levels of *C1qa*, *C1ra* and *C1s* genes were increased in the aortic tissue 1 week after AngII infusion (Fig. 8a). Aortic Mϕs increased *C1qa* gene expression, but not *C1ra* and *C1s*, 1 week after AngII infusion (Fig. 8b). Treatment with C1-INH prevented the activation of β-catenin signalling in aortic VSMCs and suppressed proliferation of VSMCs induced by AngII infusion (Fig. 8c,d; Supplementary Fig. 6a). In addition, activation of β-catenin signalling and proliferation of VSMCs were both attenuated in C1qa-deficient